Available online at www.sciencedirect.com

ScienceDirect

Geochimica et Cosmochimica Acta 286 (2020) 441–460

Geochimica et Cosmochimica Acta

www.elsevier.com/locate/gca

Elucidating the processes affecting highly primitive lavas of the Borgarhraun flow (northern Iceland) using trace elements in olivine

Peter Tollan [a,b,c,*], Andrey Gurenko [d], Jörg Hermann [a]

[a] Institut für Geologie, Universität Bern, Bern, Switzerland
[b] Research School of Earth Sciences, The Australian National University, Canberra, Australia
[c] Institute of Geochemistry and Petrology, ETH Zürich, Zürich, Switzerland
[d] Centre de Recherches Pétrographiques et Géochimiques, Université de Lorraine, France

Received 10 February 2020; accepted in revised form 22 July 2020; available online 30 July 2020

Abstract

Olivine is typically the first phase to crystallise from basaltic melts and its chemistry can therefore inform on the earliest stages of magmatic evolution, not recorded by later crystallising phases. Despite the potential of olivine for understanding primitive differentiation, limited analytical capabilities have previously restricted the range of elements that can be routinely measured. Consequently, important processes controlling early magma evolution may have been overlooked or misidentified. This study reports a wide range of minor and trace elements in forsteritic (up to $Fo_{92.2}$) olivine macrocrysts from the primitive Borgarhraun lava flow in northern Iceland.

We define two distinct populations of olivine based on their forsterite (Fo) content and then apply minor and trace element data to discern mixing and crystallisation of subtly different high-MgO parental melts. High-Fo (90.9–92.2 mol%) olivines show approximately linear trends between Cr and other incompatible trace elements (Li, Na, Ca, Ti, Al and Y), implying mixing and concurrent crystallisation of two highly primitive melts. Low-Fo (87.4–90.0 mol%) olivines show trends that indicate mixing and crystallisation of multiple, genetically distinct and less primitive melts. The outermost 50 μm of the olivine microcrysts record diffusive re-equilibration of the olivine macrocrysts to a single, significantly more evolved carrier liquid over an ascent timescale of 70–250 days. Compared to the rest of Iceland, the Borgarhraun olivine macrocrysts are distinguished by their Cr contents, which extend from 97 to 1150 ppm. The uniquely steep trend in Fo vs. Cr can be explained by early crystallisation of Cr-spinel and Cr-rich clinopyroxene, stabilised by high pressures of differentiation (>0.8 GPa). Chromium-forsterite systematics may therefore be a powerful tool for qualitatively assessing relative pressures of crystallisation for different magmatic systems. Collectively, our new dataset clearly demonstrates the importance of measuring trace elements in olivine for identifying the formative stages and conditions of basaltic magmatic systems.

Keywords: Olivine; Trace element; Primitive; Basalt; Differentiation; Iceland

1. INTRODUCTION

The application of basalt geochemistry to determining the nature of the underlying mantle source is challenging, since modification by cooling, crystallisation, cumulate recycling and mixing with more evolved melt compositions

* Corresponding author at: Institut für Geologie, Universität Bern, Bern, Switzerland.
E-mail address: peter.tollan@erdw.ethz.ch (P. Tollan).

https://doi.org/10.1016/j.gca.2020.07.033
0016-7037/

occurs rapidly and almost ubiquitously during crustal residence and eruption. This is readily apparent from detailed geochemical and isotopic studies of crystal and glass constituents of lavas and cumulates, and by studies of bulk-rock heterogeneity within individual lava flows (Slater et al., 2001, Stracke et al., 2003a, Dungan and Davidson, 2004; Costa and Dungan, 2005; Davidson et al., 2007; Maclennan et al., 2003a; Maclennan, 2008a; O'Neill and Jenner, 2012; Neave et al., 2013). Melt inclusions are often used as proxies for the liquid in equilibrium with their crystal host. However, syn- and post-entrapment processes can result in melt inclusion compositions that poorly represent the parental melt composition and which can be hard to identify, particularly given the small analytical volume of typical basaltic melt inclusions (Danyushevsky et al., 2000; Danyushevsky et al., 2004; Spandler et al., 2007; Kent, 2008; Baker, 2008). Alternatively, the composition of crystal phases generated by early stages of crystallisation can be used as tracers of primary melts (Sobolev et al., 2007; Herzberg, 2011; Foley et al., 2013; Tollan et al., 2015; Neave et al., 2018). Olivine and spinel are particularly appropriate for this goal, since they are typically the first two liquidus phases during crystallisation of high-Mg melts. Whilst the compositions of the crystals cannot truly reflect primary melts, they may very closely approximate them, since small degrees of spinel and olivine fractionation have little effect on the chemical composition of the melt other than the few elements that are strongly enriched in these phases (namely, Mg and Ni in olivine, Cr in spinel). Modification of the chemical composition of early crystallising olivine and spinel can occur through dissolution/recrystalli zation, crystal growth and solid-state diffusion, however these processes are both readily identified petrographically and analytically (Costa and Dungan, 2005; Shea et al., 2015; Mutch et al., 2019a). Hence, olivine with high, mantle-like forsterite (Fo) contents (calculated as $100 * Mg/(Mg + Fe)$ in molar proportions) have been considered as reliable proxies for primitive mantle-derived melts (Ruprecht and Plank, 2013).

Traditionally, a major obstacle of using olivine to inform complex petrogenetic processes has been its relatively simple chemistry, particularly the inability to incorporate quantifiable amounts of many incompatible trace elements, such as the rare earth elements (REE). The analytical challenges presented by this has led to a bias towards other crystal phases (e.g., clinopyroxene and plagioclase) that more readily incorporate these elements. These phases, however, fractionate after the onset of olivine crystallisation, meaning they are unable to document the earliest evolution of mantle-derived melts. Consequently, a number of recent studies have strived to develop the quantification of, and interpretative framework for, an expanded range of trace elements in olivine (De Hoog et al., 2010; Foley et al., 2013; Mallmann and O'Neill, 2013; Bouvet de Maisonneuve et al., 2016; Stead et al., 2016; Neave et al., 2018; Tollan et al., 2018; Bussweiler et al., 2019). For example, several highly incompatible elements (e.g., Ti, Y, Zr and Yb) are well within the analytical capabilities of modern laser-ablation mass spectrometry (LA-ICP-MS) and secondary ionisation mass spectrometry (SIMS). Combined with Ni, Ca, Co, Al, Cr, Na, Li, Sc, V and P elements with a wide range of chemical affinities can now be routinely measured in olivine. This opens up new possibilities to apply trace elements in olivine to develop new understanding of the behaviour of basaltic magmas.

In this contribution, we document a detailed *in-situ* geochemical study of the most magnesian olivine (up to $Fo_{92.2}$) known so far for the recent, highly primitive Icelandic tholeiites from northern Iceland (Polyakov et al., 1976; Gurenko et al., 1988). We use single spot and profile analyses of trace, minor and major element for ~80 olivine grains to constrain the major petrogenetic proesses for near-primary Icelandic magmas. Our key finding is that Cr, combined with other trace and minor elements such as Li, Na and Y, documents very early, new melt mixing trends within highly forsteritic olivine macrocrysts, not apparent from other phases within the lava assemblage. The trace elements, particularly Cr, reveal that the composition of even highly forsteritic olivine may have been impacted by extensive early melt modification processes, which are not identifiable using major and minor elements alone. Trace element analyses of olivine are, therefore, a powerful and essential tool for the interpretation of the origin of primitive basalts.

2. SAMPLE LOCALITY AND PETROGRAPHY

The sample (11,898) studied here comes from the post-glacially erupted Borgarhraun lava flow (7–12 Ka), part of the Theistareykir volcanic field in northern Iceland (~2.5 km to the north-west from the Bæjarfjall table mountain on the south-west slope of the small, 370 m above sea level Stórihver eruption unit; Fig. 1; Polyakov et al., 1976; Gerasimovsky et al., 1978; Gurenko et al., 1988). The sample is pristine and has a complex texture (Fig. 2), consisting of a seriate groundmass (continuous grain size distribution) comprised of olivine, clinopyroxene and plagioclase crystals (<50 to ~200 μm). Dispersed within this matrix are abundant macrocrysts of olivine (~0.5–2 mm). Skeletal titanomagnetite is frequently observed, along with scarcer crystals of Cr-spinel. The olivine macrocrysts have anhedral-subhedral crystal shapes, and contain frequent inclusions of Cr-spinel and glass (the latter generally partially or completely re-crystallised). The macrocrysts look essentially homogenous with respect to major elements, as seen in the backscattered electron images, with only the outermost 50 μm displaying brighter contrast, suggesting Fe enrichment. The Borgarhraun lava flow is known for displaying substantial textural and geochemical variability down to hand-sample scale (Maclennan et al., 2003a, 2003b). The textures displayed by the sample studied here are consistent with the description of coarse textures in the massive interior of the flow (Maclennan et al., 2003b). Although the texture of the sample studied here is not representative of the entire flow, as is discussed later, the occurrence of olivine macrocrysts and the distribution of their compositions are entirely consistent with previous studies, which utilised more complete sampling of Borgarhraun (Maclennan et al., 2003b; Thomson and Maclennan, 2013).

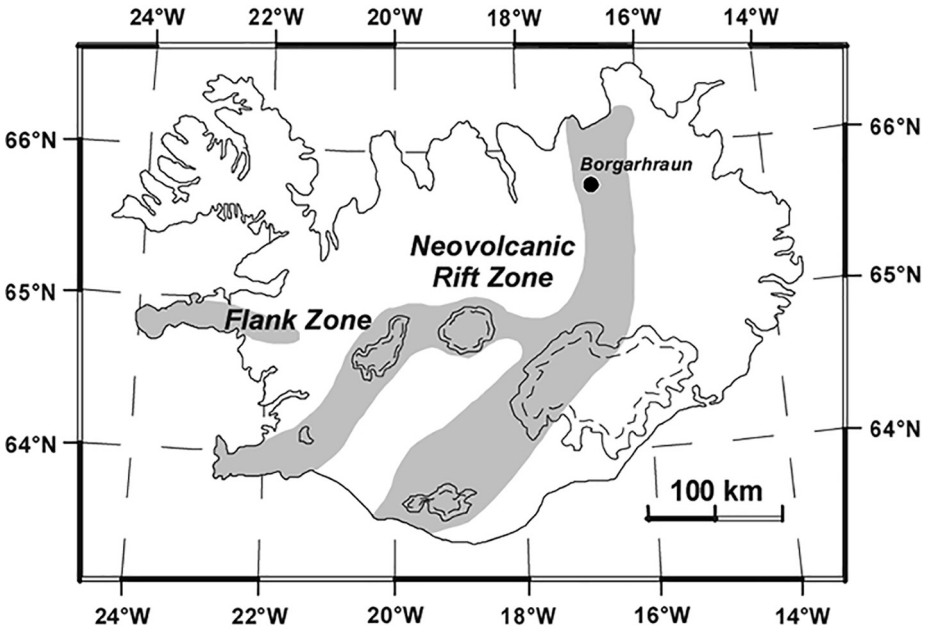

Fig. 1. Map of Iceland showing the location of the Borgarhraun lava flow.

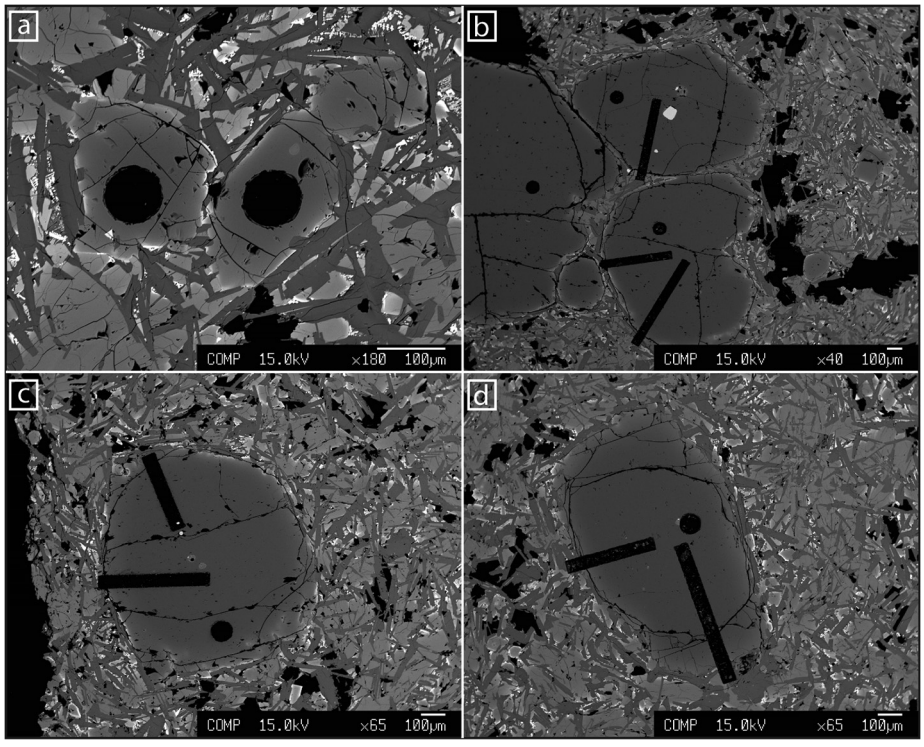

Fig. 2. Backscatter SEM images of olivine macrocrysts in their crystalline matrix (plagioclase, clinopyroxene, olivine, titanomagnetite). Bright inclusions are Cr-spinel. Dark circles and lines and LA-ICP-MS spots and line profiles respectively.

3. PREVIOUS STUDIES ON BORGARHRAUN

Numerous previous studies investigating the Borgarhraun volcanic field have utilised whole-rock chemical compositions of lavas, the major element composition of olivine, the major/trace element composition of clinopyroxene and the major and trace element composition of olivine-hosted melt inclusions to determine the composition of least differentiated primitive melts and physico-chemical (namely, pressure, temperature and oxygen fugacity-P-T-

fO_2) conditions of their generation and later modification (Polyakov et al., 1976; Gurenko et al., 1988; Slater et al., 2001; Maclennan et al., 2003a, 2003b; Stracke et al., 2003a; Maclennan, 2008a, 2008b; Winpenny and Maclennan, 2011; Thomson and Maclennan, 2013; Matthews et al., 2016). These studies have collectively demonstrated that the high- and low-Fo olivines and their inclusions may reflect concurrent mixing and fractional crystallisation of at least two primitive melts. For example, decreasing La/Yb variability of melt inclusions with decreasing host olivine Fo content was interpreted to represent progressively greater degrees of melt mixing and compositional homogenisation during magma cooling and fractional crystallisation (Maclennan et al., 2003a). The highest Fo olivine population ($Fo_{91–92}$) however is distinct in only trapping the melts with relatively low La/Yb. Maclennan et al. (2003a) and Maclennan et al. (2003b) interpreted this to indicate crystallisation from primitive melts formed by high degrees of melting at relatively shallow depths. Maclennan (2008a) used ratios of REE to show that the degree of melt mixing decreased with decreasing Fo content within this olivine population. The timescales associated with the crystallisation, storage and eruption of the Borgarhraun magmas were assessed by major element concentration profiles in olivine and spinel from wherlitic nodules included within the lava flow (Mutch et al., 2019a, 2019b). These studies have demonstrated that crystallisation and storage of crystals derived from primitive melts occurred over relatively short timescales of ~1000 years (Mutch et al., 2019a), while scavenging and eruption of olivine macrocrysts from these deep crystal-rich magma reservoirs occurred within a few weeks (Mutch et al., 2019b).

4. METHODS

The hand sample was prepared into two thin sections for categorisation by microscopy and geochemical analysis. Additional olivine macrocrysts were also separated from the matrix and mounted in epoxy resin for analysis. Major element concentrations of olivine and spinel were determined by electron microprobe at the Institute of Geological Sciences, University of Bern, using a JEOL JXA-8200 using a standard analytical routine for silicates. The accelerating voltage and the beam current were 15 kV and 20 nA, respectively. Counting times were 10 s on the background on each side of the peak and 20 s on the peak. Standardisation was performed using a suite of reference materials for electron probe microanalysis consisting of natural and synthetic crystals of anorthite (Al), albite (Na), spinel (Cr), wollastonite (Ca), olivine (Si, Mg), ilmenite (Ti), almandine (Fe), tephroite (Mn) and bunsenite (Ni). Trace and minor element concentrations were determined by LA-ICP-MS at the Research School of Earth Sciences, The Australian National University (ANU) and the Institute of Geological Sciences, University of Bern. At ANU, an Agilent 7700 quadrupole ICP-MS was coupled to an in-house laser ablation setup, consisting of a Coherent COMPex 110 Excimer (193 nm) laser and two-volume ablation chamber. The diameter of the spot was 62 μm, and a laser repetition rate of 5 Hz and a fluence of ~6 J/cm^2 were used. Ablated material was delivered to the ICP-MS in a gas mixture consisting of He, Ar and H. A signal-smoother was employed to eliminate pulses in the measured signal due to the rapid washout rate of the ablation chamber. The isotopes measured were ^{7}Li, ^{23}Na, ^{25}Mg, ^{27}Al, ^{29}Si, ^{31}P, ^{43}Ca, ^{45}Sc, ^{47}Ti, ^{51}V, ^{53}Cr, ^{55}Mn, ^{57}Fe, ^{59}Co, ^{60}Ni, ^{61}Ni, ^{63}Cu, ^{65}Cu, ^{89}Y and ^{90}Zr, with individual counting times of 0.01–0.2 seconds for a total acquisition cycle of 0.52 seconds. NIST 610 and NIST 612 were used as a primary calibration standards (Jochum et al., 2011), with BCR-2G as a secondary standard, and Iolite as data reduction software (Paton et al., 2011).

At the University of Bern, trace element concentrations were acquired using an Agilent 7900 ICP-MS coupled to an Australian Scientific Instruments (193 nm) RESOlution laser ablation system. Spot measurements were conducted under identical conditions as at ANU, except for the use of a slightly larger spot (80 μm) and the addition of a small amount of N to the carrier gas, rather than H. Additional measurements of rare earth elements (REE) were conducted on a subset of olivine macrocrysts. These measurements utilised a 100 μm spot, 10 Hz repetition rate and a fluence of 7 J/cm^2. Counting times on ^{175}Lu, ^{172}Yb, ^{169}Tm, ^{166}Er, ^{165}Ho, ^{163}Dy and ^{159}Tb were 0.1 s. All other REE were below the limits of detection. Chromium was added to the routine to ensure data consistency between the two sets of measurements, in addition to Si and Mg. Line profiles were measured using a rectangular slit with a dimension of 10x50 μm, which was moved at a constant speed of 1 μm/second, from the core to just outside the rim of each crystal (Supplementary Fig. 2). Care was taken to ensure that the long axis of the slit was approximately parallel with the rim of the crystal. The profiles were always placed so as to avoid fractures and only done in crystals where the rim-matrix contact was well preserved, thereby ensuring that the concentrations of the crystal rims could be accurately determined. A cleaning run at 10 μm/second and 10 Hz was performed before each analysis. The elements measured were ^{7}Li, ^{23}Na, ^{25}Mg, ^{27}Al, ^{29}Si, ^{31}P, ^{43}Ca, ^{47}Ti, ^{53}Cr, ^{57}Fe, ^{60}Ni and ^{89}Y. The total acquisition cycle was 2.132 seconds, therefore generating a new datapoint for every 2.132 μm of horizontal movement. Repetition rate and fluence were 10 Hz and 4 J/cm^2 respectively. Standards measured for both spot and line profiles were NIST 612 (calibration standard), GOR132, KL2 and BHVO-2G. Line profiles were calibrated against spot measurements on the same crystal by normalising the core measurements to an adjacent spot measurement and then adjusting the remaining profile by this ratio.

An important consideration of such small laser profiles is how precisely the rim composition can be measured. The dimension of the slit used in the laser line profiles was 10x50 μm. Hence, when the slit was positioned perfectly at the rim of the crystal an average of the outermost 10 μm was obtained. As a result, it was not possible to precisely measure the concentration immediately adjacent to the crystal-groundmass boundary. To compensate for this, we assumed that the outermost laser point represents 5 μm from the crystal rim (the centre of a 10 μm slit that is perfectly aligned with crystal-groundmass interface). The

concentration of the rim at the crystal-groundmass interface was then calculated by fitting the profiles to the following equation for 1D diffusion in a semi-infinite body:

$$C(x) = C_0 - (C_0 - C_i)\mathrm{erf}\left(\frac{x}{2\sqrt{Dt}}\right)$$

where $C(x)$ is the concentration of an element at distance x from the crystal-melt interface, C_0 is the concentration at the crystal rim, C_i is the initial concentration in the olivine, D is the element diffusivity in olivine, and t is the time over which diffusion occurs. For the purpose of this exercise, arbitrary values of D and t were selected and a least squares regression method was used to solve for the rim concentrations.

5. RESULTS

The Forsterite (Fo) contents of Borgarhraun olivine macrocryst cores range from 92.2 to 87.4 mol%, consistent with the previous analyses of olivine from this sample by Gurenko et al. (1988) (Fig. 3; Table 1; Supplementary data). As has been well-established by previous studies on Borgarhraun (Maclennan et al., 2003a, 2003b; Thomson and Maclennan, 2013; Matthews et al., 2016), this range of macrocryst compositions is approximately bimodal, with two groups with $Fo_{92.2–90.9}$ and $Fo_{90.0–87.4}$. The trace and minor element concentrations acquired by LA-ICP-MS for this study establish much more clearly the modality of olivine populations. Several elements (most notably Li, Na, Al, Ca, Cr and Y) display a systematic difference between the high- and low-Fo populations (Figs. 3 and 4). This distinction is apparent from a combination of the absolute concentrations of these elements, the generally greater variability in concentrations and the tendency to form correlations with Fo contents, specifically for olivines from the high-Fo group (Figs. 3 and 4). Chromium, in particular, shows a remarkably wide range of concentrations, from 97 to 1150 ppm. When plotting the concentrations of different trace and minor elements against each other, the low-Fo olivine macrocrysts are generally poorly

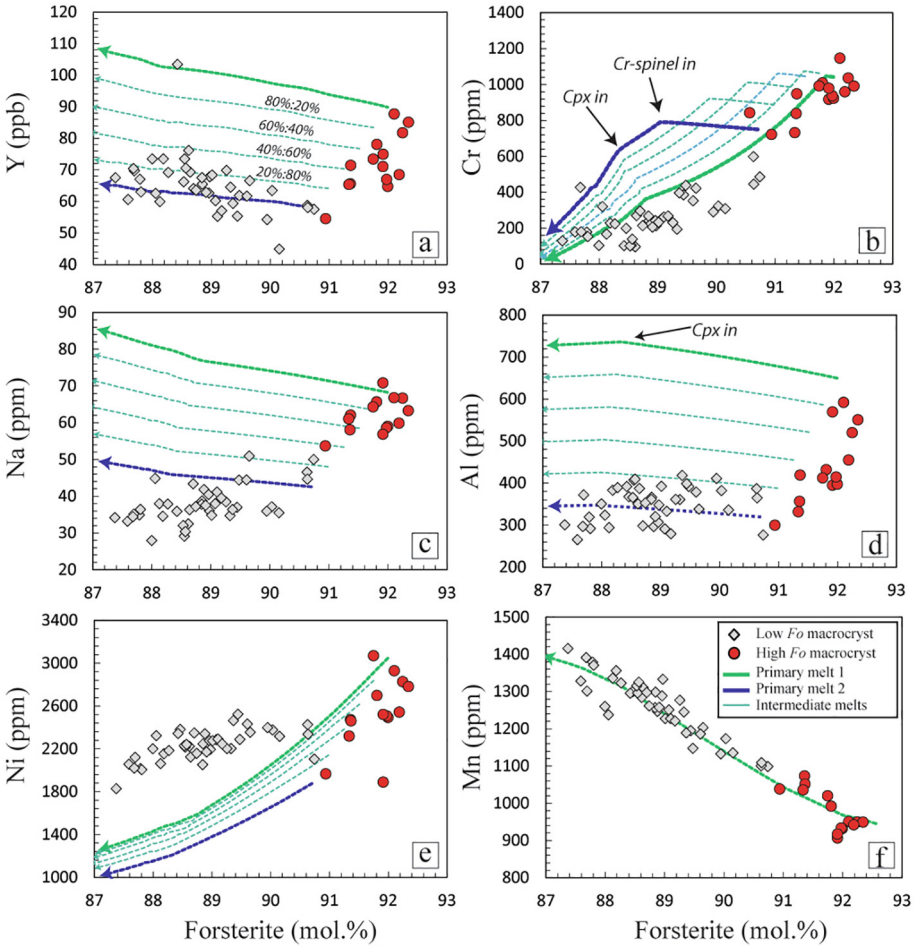

Fig. 3. Relationships between Fo and minor/trace elements in olivine macrocrysts and groundmass olivine. Data are for crystal cores. Crystal rims are largely homogeneous and represented in subfigures e and f by a purple star. Uncertainties are similar or smaller than the symbol sizes. Dark green and blue arrows represent the results of of PETROLOG fractional crystallisation modelling (Danyushevsky and Plechov, 2011) of melt compositions 1 and 2 respectively (Table 2). Pale green lines represent mixtures of these two primary melts followed by fractional crystallisation. Note that the model for Mn was produced by subtracting measured mineral compositions from the starting melt composition (see Appendix A and supplementary data for explanation and calculation).

Table 1
Extreme (highest and lowest) and average major, minor and trace element compositions of the high and low olivine macrocrysts and groundmass olivine. The full range of compositions can be found in the Supplementary Data.

	High forsterite group				*Low forsterite group*				*Matrix*	
	Max Fo	Min Fo	Average	1 s.d.	Max Fo	Min Fo	Average	1 s.d.	Max Fo	Min Fo
SiO_2	40.61	40.51	40.67	0.20	40.51	40.03	40.18	0.23	38.89	33.50
TiO_2	b.d.l.	b.d.l.	b.d.l.	b.d.l.	b.d.l.	b.d.l.	b.d.l.	b.d.l.	b.d.l.	0.14
Al_2O_3	0.17	0.10	0.11	0.08	0.04	0.13	0.07	0.04	0.08	0.05
Cr_2O_3	0.16	0.12	0.13	0.02	0.09	0.01	0.04	0.02	0.03	0.00
FeO	7.52	9.30	8.12	0.50	9.05	12.06	10.80	0.77	18.74	49.07
MnO	0.12	0.15	0.14	0.01	0.14	0.20	0.17	0.02	0.30	0.72
MgO	50.18	50.07	50.45	0.57	49.75	46.81	48.45	0.74	42.29	16.85
CaO	0.35	0.37	0.39	0.06	0.45	0.36	0.34	0.03	0.38	0.44
NiO	0.40	0.32	0.33	0.04	0.29	0.23	0.28	0.03	0.17	0.02
Total	99.51	100.93	100.33	0.64	100.32	99.84	100.33	0.50	100.87	100.80
Fo (mol.%)	92.2	90.6	91.7	0.5	90.7	87.4	88.9	0.8	80.1	38.0
Li	1.20	1.22	1.22	0.06	1.17	0.96	1.00	0.12		
Na	66.7	53.6	61.4	5.0	50.0	34.2	37.9	5.1		
Al	520	376	435	87	277	301	349	42		
P	27.1	19.2	26.4	18.5	n.a.	47.4	33.0	20.7		
Ca	2003	2499	2383	267	3001	1921	2162	205		
Sc	8.55	6.33	7.22	1.37	10.08	9.30	8.23	1.42		
Ti	19.7	15.5	17.0	2.6	15.4	21.0	18.6	2.9		
V	8.71	7.46	7.94	0.69	7.67	9.04	8.73	0.92		
Cr	1036	843	932	111	487	130	259	115		
Mn	950	1072	985	59	1099	1416	1260	80		
Co	136	144	135	5	131	184	168	9		
Ni	2828	2557	2537	318	2104	1829	2234	141		
Y (ppb)	82	59	71	9.3	57	68	65	8.7		
Tb (ppb)	0.6	n.a.	0.5	0.1	0.4	0.4	0.5	0.1		
Dy (ppb)	8.7	n.a.	7.0	1.3	6.2	6.5	6.4	0.6		
Ho (ppb)	3.0	n.a.	2.4	0.4	2.2	2.3	2.3	0.2		
Er (ppb)	14.5	n.a.	11.7	1.8	10.7	11.6	11.3	1.0		
Tm (ppb)	3.1	n.a.	2.5	0.4	2.3	2.6	2.6	0.2		
Yb (ppb)	30	n.a.	25	3.5	22	26	25	2.3		
Lu (ppb)	6.3	n.a.	5.3	0.8	4.7	5.5	5.4	0.5		
Zr (ppb)	8.7	15.3	10.5	3.6	6.6	9.5	9.4	2.9		

correlated, whereas the high-Fo olivines show multiple strong correlations (Fig. 4). Often these correlations are in the opposite sense to correlations in the low-Fo group (where present). This is particularly apparent when Cr is plotted against other trace/minor elements, such as Y, Na, Ca, Al and Li (Fig. 4a-e), or in a plot of Y vs. Na (Fig. 5b). Nickel concentrations (Fig. 5a) vary more in the high-Fo population (1800–3100 ppm) compared to the low-Fo population (2000–2600). Rare earth elements (Lu to Tb) range in concentration from 0.4 ppb (Tb) to 30 ppb (Yb). Primitive mantle-normalised REE patterns for olivines from the two populations are similar, showing a steep downwards dipping pattern from Lu to Tb (Fig. 6). The ratio Dy/Lu shows subtle differences between the two olivine populations when plotted against Fo, Zr and Cr (Fig. 6).

High resolution LA-ICP-MS profiles from core to rim show that the macrocrysts from both high and low-Fo populations are relatively homogenous until the outermost rim, which is ~50 μm wide (Figs. 7 and S1 – *Supplementary data*). Phosphorous can show more substantial, non-systematic variations in concentration, which are not reflected in the concentration profiles of other elements (Fig. S2 – *Supplementary data*). The outermost 50 μm, however, show concentration profiles in almost every element, with the notable exception of Al. Crystals with distinct core compositions converge towards a single rim composition for most elements (Fig. 7). This is most striking for Cr, Co, Mn and Ni. Of these, Cr is particularly unique. High-Fo olivines start with exceptionally Cr-rich cores (~1000 ppm) and then decrease to a rim concentration of ~200–400 ppm. Low-Fo olivines display more complex, sinusoidal profiles. The cores are relatively Cr-poor (~200 ppm), then approximately 20–40 μm from the rim, the concentration increases, before decreasing again slightly in the outermost 20 μm. Highly incompatible trace element (e.g., Ti and Y) profiles have rim concentrations that are different to any of the olivine macrocryst cores (Fig. 7e and g). For example, the olivine cores have a range of Y concentrations from 45-105 ppb, whereas the rims are substantially enriched (~200–300 ppb). Highly incompatible trace elements also display less convergence at the rim than more compatible minor/trace elements. For example, projected rim concentrations of Ti range from 38-70 ppm, whereas the cores vary less (12–26 ppm). Fo content converges to ~78–80 mol%.

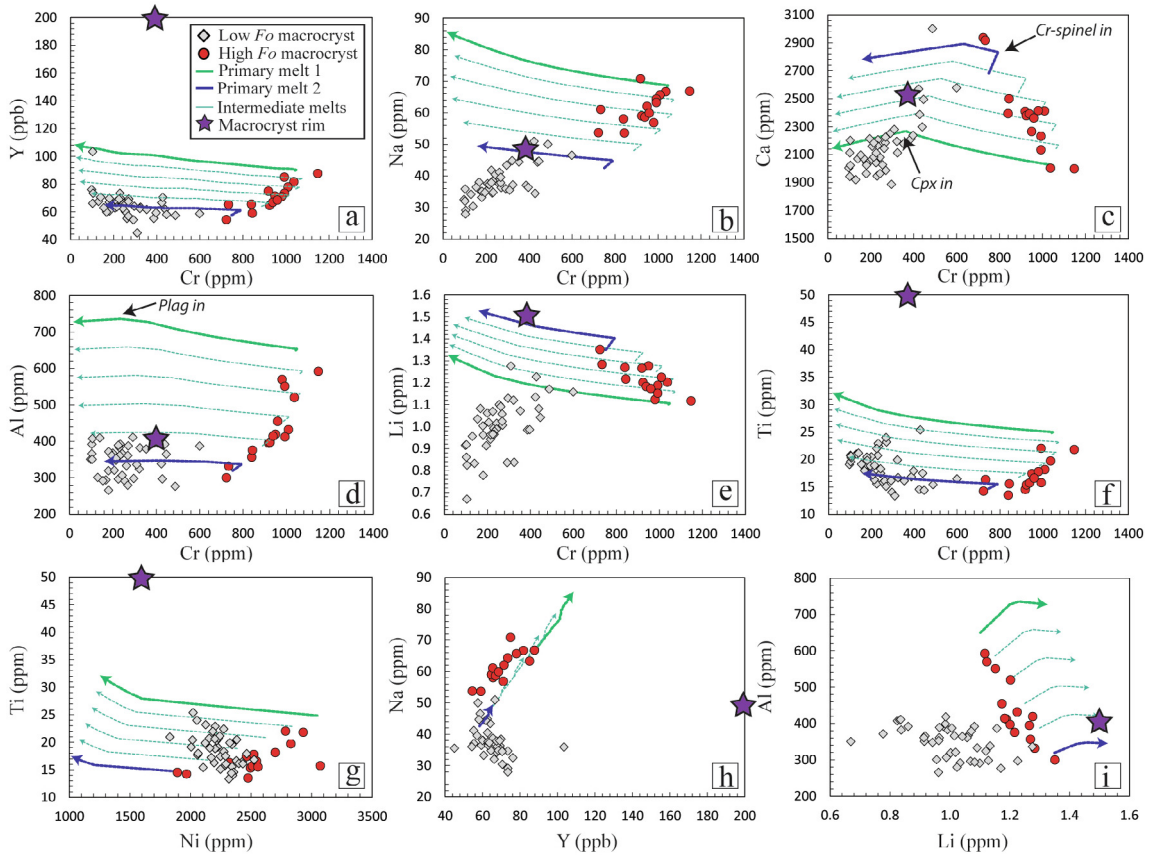

Fig. 4. Relationships between trace elements measured in olivine macrocryst cores by LA-ICP-MS. Crystal rims are largely homogeneous and represented by purple stars. Uncertainties are similar to or smaller than the symbols (see Table 1 and Supplementary Data). Dark green and blue arrows represent the results of PETROLOG fractional crystallisation modelling (Danyushevsky and Plechov, 2011) of melt compositions 1 and 2 respectively (Table 2). Pale green lines represent mixtures of these two primary melts followed by fractional crystallisation. The appearance of phases is marked in subfigures c and d.

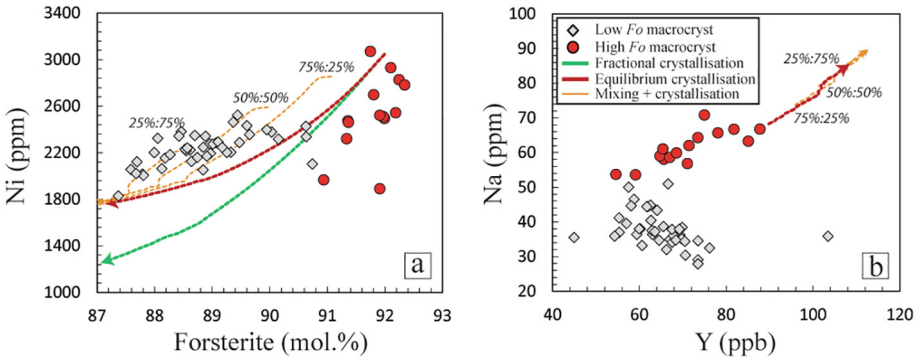

Fig. 5. Results of equilibrium crystallisation and mixing models for Ni-Fo and Na-Y. Models are constructed in PETROLOG (Danyushevsky and Plechov, 2011) and compared to fractional crystallisation for reference. Note that in subfigure b the fractional crystallisation model is not plotted since it overlaps too closely with the other models. Mixing models were created by mixing the differentiated starting melt with the original melt composition in different proportions and then allowing to crystallise.

Similar to the macrocrysts, groundmass olivine displays an approximately bimodal distribution of chemical compositions, as determined by electron microprobe (Fig. S3 – *Supplementary data*). One, relatively less evolved olivine population has a Fo content of 67–80 mol%, NiO of 0.10–0.17 wt.% and MnO of 0.30–0.49 wt.%, whereas the second, more evolved population has a Fo content of 38–52 mol%, NiO of 0.02–0.09 wt.% and MnO of 0.60–0.72 wt.%. The TiO_2 contents range from <0.01 to 0.14 wt.% (equal to <100–850 ppm Ti) and negatively correlate with

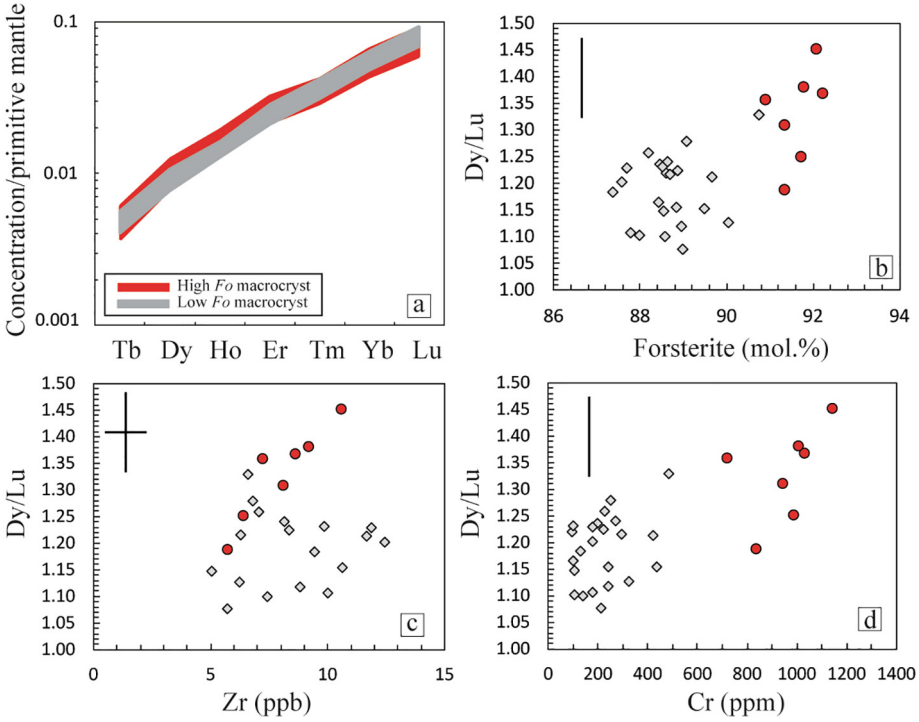

Fig. 6. Subfigure a compares normalised REE concentrations in high- and low- Fo olivine macrocryst populations. The shaded areas represent the full range of values in each population. Primitive mantle values are from Palme and O'Neill (2013). Subfigures b, c and d compare Dy/Lu ratios with Fo content, Zr and Cr concentrations. 1sd uncertainty in trace element ratios is given by a black vertical and horizontal bars.

Fo (Fig. S3 – *Supplementary data*). Substantial zoning of larger groundmass olivine is evident, with rims depleted in Ni and enriched in Fe, Mn and Ti.

Olivine-hosted spinel inclusions (Fig. S4 – *Supplementary data*) from the high-Fo group are more abundant and have higher Cr# (Cr# = Cr/(Al + Cr))between 0.53 and 0.61), as compared to those from the low-Fo group (Cr# = 0.20–0.22). Mg# (Mg# = Mg/(Mg + Fe)) is similar for the two populations, but tends to vary more in the high Cr# spinels. TiO_2 is higher in the high Cr# population (0.19–0.23 vs. 0.14–0.15 wt.%). There are generally good correlations between the concentrations of elements in the spinel inclusions and their olivine hosts (Fig. S5 – *Supplementary data*, as well as between Mn in spinel and particular trace/minor elements in the host olivine (namely Na, Cr and Y). Chromium-spinel of the groundmass is rare and has Cr# of 0.44–0.50, Mg# of 0.48–0.56 and high TiO_2 of 0.26–0.37 wt.%.

6. DISCUSSION

6.1. Thermometry

The good correlations between the chemistry of spinel inclusions and the adjacent host olivines indicate that both phases are in equilibrium (Fig. S5 – *Supplementary data*), and hence element exchange thermometers can be applied to determine equilibration temperature. We selected the Al-exchange thermometer of Coogan et al. (2014), a modified version of the thermometer of Wan et al. (2008). The popularity of this thermometer for determining liquidus temperatures of basaltic melts stems from a combination of the pressure insensitivity, independence from melt composition and the assumption that Al diffuses slowly in olivine, permitting the preservation of concentrations reflective of liquidus temperatures (Coogan et al., 2014; Spandler and O'Neill, 2010; Heinonen et al., 2015; Matthews et al., 2016; Sobolev et al., 2016; Spice et al., 2016; Jennings et al., 2019). The assumption of slow diffusivity was based on limited experimental data from Spandler and O'Neill (2010), who showed that at the conditions and starting compositions of their experiments, the rate of Al diffusion in olivine was several orders of magnitude slower than other elements. More recently, Zhukova et al. (2017) and Le Losq et al. (2019) have demonstrated that a second, faster pathway of Al diffusion exists (comparable to rates of Fe-Mg inter-diffusion), which is favoured by conditions of higher silica activity.

In the case of the samples studied here, the preservation of a wide range of Al concentrations in both the macrocryst cores, combined with the lack of any systematic core-rim zoning and homogeneous rim concentrations, indicates minimal reequilibration of Al concentrations by diffusion. Note that this is contrary to the Borgarhraun samples studied by Matthews et al. (2016) and, in particular, Mutch et al. (2019b), who found distinct zoning in Al at olivine rims, interpreted to reflect crystal growth rather than diffusion. One final consideration for Al exchange thermometry

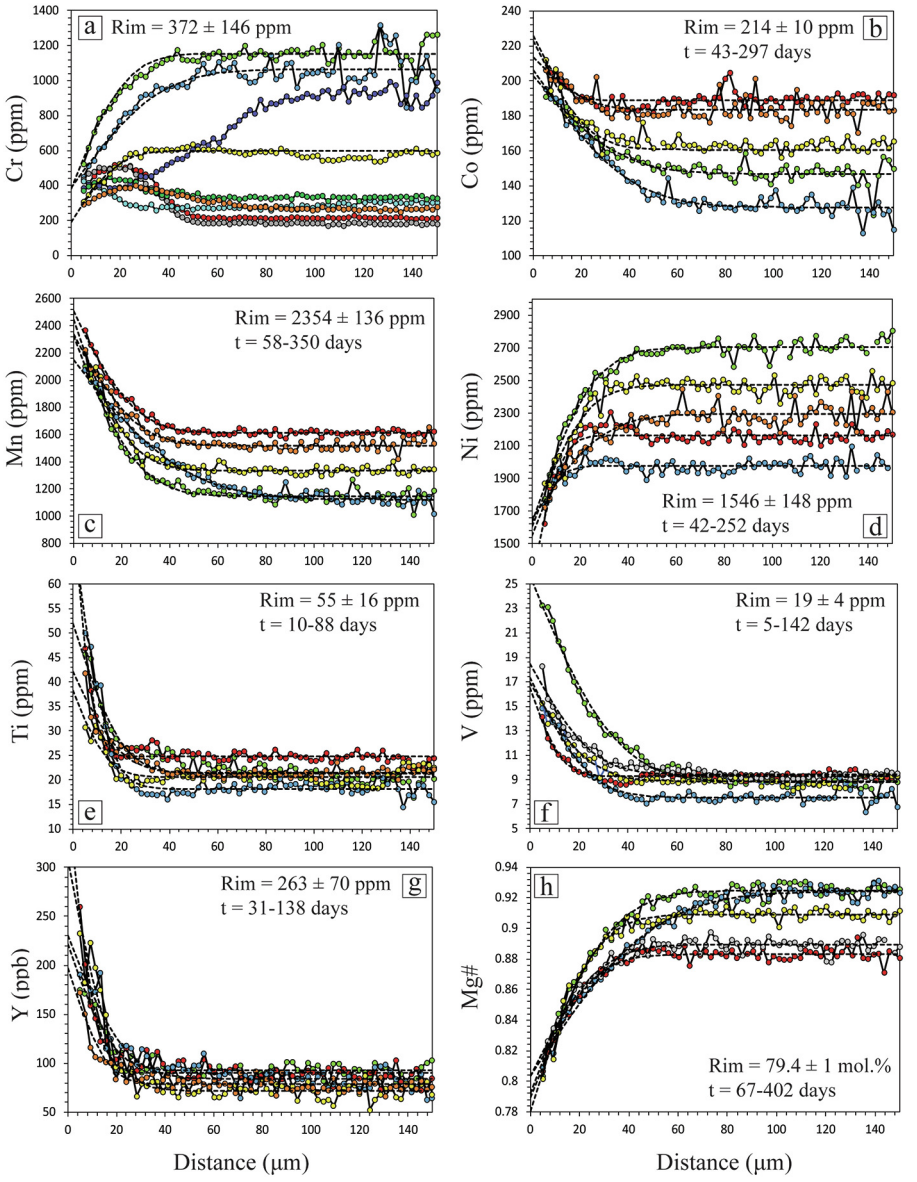

Fig. 7. Results of LA-ICP-MS line profiles towards the crystal-groundmass interface. Rim concentrations are an average of all measured profiles. Model curves and timescales are the results of diffusion modelling (see Section 6). Each data point corresponds to the acquisition time for the element list (2.132 seconds). Line profile scanning rate was 1 μm/s. Full details are provided in the methods section.

is the potential for Al solubility and diffusion mechanism to be affected by the presence of monovalent cations (particularly Na, but also H and Li). These have been shown to charge balance trivalent cations in natural olivine (Tollan et al., 2018), although further work is needed to rigorously test such charge-balancing effects.

For the calculation of Al-exchange temperature, LA-ICP-MS measurements of Al in olivine were combined with EPMA data for Al_2O_3 and Cr_2O_3 in spinel. Use of LA-ICP-MS data for Al in olivine was preferred because of the greater precision compared to the equivalent EPMA data. The accuracy of the LA-ICP-MS data was established by repeat measurements of the secondary standard BCR-2G, returning values within 2% of the accepted value (Jochum et al., 2005). Precision of Al in olivine measurements using this LA-ICP-MS setup was established over multiple sessions using an in-house standard of San Carlos olivine (Tollan et al., 2018), which returned a value of 3.7% RSD (94 ± 4 ppm). Using this dataset, calculated equilibrium temperatures are 1330–1410 °C and 1250–1260 °C for the high- and low-Fo groups respectively (Fig. S4b – *Supplementary data*). These results are in good agreement with the previous, pioneering microthermometry study of melt inclusions from this sample (1330–1200 °C; Gurenko et al., 1988) and the study on Borgarhraun of Matthews et al. (2016), who employed the same thermometer but utilised high precision EPMA data for both olivine and spinel Al and Cr concentrations. The high-Fo population in this

study extends to slightly lower temperatures than the population measured by Matthews et al. (2016), however this is consistent with the generally less primitive compositions of the spinel inclusions measured in this study (Fig. S4 – *Supplementary data*).

6.2. Origin of the high-Fo olivine macrocrysts

The high-Fo olivines are distinguished by correlations between different trace/minor elements and Fo content (Figs. 3 and 4), trends which are (with the occasional exception) absent from low -Fo olivines. These data clearly indicate a unique history for each of these two olivine populations. Considering just the high-Fo population, there are two main options for explaining the observed trends: crystallisation of a single primary melt, or mixing of two primary melts combined with cooling and crystallisation. In order to test which of these options can best explain the data, a range of crystallisation models were generated using the software PETROLOG (Danyushevsky and Plechov, 2011). Two primary melt compositions were used in the model calculations (Table 2). The first was taken from Shorttle and Maclennan (2011) and Matthews et al. (2016), and is in equilibrium with Fo_{92} (the most forsteritic olivines from the high-Fo group). A second primary melt was created to be in equilibrium with the least forsteritic olivines from the high-Fo group (Fo_{91}), by removing equilibrium olivine in 0.01% steps from the first primary melt. We note that using the very similar primary melt composition from Gurenko et al. (1988) has no significant impact on the model results or their subsequent interpretation.

Table 2
Starting melt compositions and partition coefficients used in the crystallisation models. Intermediate mixed melts are all produced from mixtures of these two compositions are their differentiated products. Primary melt 1 is from Shorttle et al. (2015) and primary melt 2 was constructed by removing equilibrium olivine until in equilibrium with Fo_{91}. Olivine-melt partition coefficients are from Mallmann and O'Neill (2013), except Li (Spandler and O'Neill, 2010) and V (calculated from Mallmann and O'Neill, 2009). See the Appendix for further details.

	Primary melt 1	Primary melt 2
SiO_2	48.7	48.9
TiO_2	0.7	0.4
Cr_2O_3	0.30	0.12
Al_2O_3	13.9	14.4
FeO	7.1	7.4
Fe_2O_3	1.4	1.4
MnO	0.14	0.16
MgO	14.2	12.6
CaO	12.3	12.8
Na_2O	1.6	1.7
K_2O	0.05	0.05
Li ppm	3.8	4.7
V ppm	200	160
Y ppm	15	12
Ni ppm	370	200
Olivine-melt partition coefficients		
Ti	0.00595	0.00613
Cr	0.51	0.913
Y	0.00603	0.00486
Ca	0.023	0.0293
Li	0.29	0.29
Na	0.006	0.0035
Al	0.00888	0.00419
V	0.044	0.049

Although a wide range of trace elements were included in the models, particular attention was given to chromium due to its substantial concentration range in the olivine samples, clear distinctions of Cr contents between the two olivine macrocryst populations, as well as to its unique partitioning behaviour in primitive igneous systems. Although Cr is a moderately incompatible element in olivine (Hanson and Jones, 1998; Mallmann and O'Neill, 2013; Bell et al., 2014), its partitioning behaviour between the melt and the bulk crystallising assemblage varies substantially as a function of the stability of spinel, in which Cr is a major structural element. Primitive basaltic melts typically co-crystallise Cr-spinel and olivine and their order of appearance on the liquidus is in part a function of Cr content in the primary melt and oxygen fugacity (Ariskin and Nikolaev, 1996; Feig et al., 2010). Since the concentration of chromium in Cr-spinel is much higher than that in the basaltic melt, crystallisation of even minor amounts of spinel will rapidly deplete the melt in Cr. Chromium is also compatible in clinopyroxene (Mallmann and O'Neill, 2009; Le Roux et al., 2013) and hence the onset of clinopyroxene crystallisation will result in further depletion of Cr. In comparison, most other trace elements are moderately to highly incompatible both in olivine and in the bulk crystallising assemblage, at least before the onset of clinopyroxene crystallisation (McDade et al., 2003; Mallmann and O'Neill, 2013).

The details of the modelling procedure, the selection of trace element concentrations in the primary melts and selected partition coefficients are provided in the Appendix A. The results are added as trend lines in Figs 3–5. Initially we considered a simple end-member scenario of fractional crystallisation. This is unlikely to truly reflect the complexity of the primitive magmatic system feeding Borgarhraun (Stracke et al., 2003a; Maclennan et al., 2003a; Maclennan, 2008a, 2008b; Thomson and Maclennan, 2013). It does, however, provide a first order understanding of whether the trends in olivine populations are generated through crystallisation of a single melt composition, and whether melts in equilibrium with high-Fo olivines are likely to have also generated the low-Fo population. Different modelling strategies are described later.

The trends in the high-Fo group are very poorly reproduced by simple crystallisation models; in many cases, the model trends are in the opposite sense to the data trends. In particular, Ni contents in the high-Fo group vary from ~3000 ppm to ~1800 ppm at nearly constant Fo (Fig. 3e). Hence, it is not possible to reconcile the high-Fo population with any simple crystallisation scenario (equilibrium crystallisation would change the concentrations slightly, but not drastically alter the model vectors, as is required). A possible explanation for some of the trends observed is charge balancing through coupled substitutions of elements. For example, Cr can be charge-balanced by Na in

olivine (Tollan et al., 2018), which could explain the positive relationship observed between these two elements for the entire selection of Borgarhraun olivines (Fig. 4b). However, other trends are less consistent with charge balance. Chromium and Li (also Al and Li) would be expected to form a similar trend to Cr and Na, whereas the opposite trend is observed (Fig. 4e, i). Moreover, if charge balancing was the dominant process controlling trace element relationships, then the trends observed in the high-Fo olivines should also be apparent for the low-Fo olivines, which is not the case (Fig. 4). Therefore, while coupled substitutions may have contributed to some of the chemical relationships, it is likely that concurrent crystallisation and mixing of different melt compositions masked or erased most or all of these trends. Due to the approximately linear relationships, we propose that two major end-member melt compositions were involved in generating the hybrid melt from which the high-Fo macrocrysts crystallised. As these two end-member melts mixed, the composition of olivine precipitating converged on an intermediate value, forming the observed compositional trends within the high-Fo population. We cannot discount the possibility that these end-member melts themselves are not the products of melt mixing; in fact, this is highly probable given the fractional mantle melting process operating beneath Iceland, which results in immediate mixing of instantaneous melts upon segregation from the mantle source (Maclennan et al., 2003a, 2003b, Stracke et al., 2003a; Maclennan, 2008a; Neave et al., 2018). Incomplete homogenisation of these true primary melt batches may help to explain some of the scatter around the mixing trends.

6.3. Origin of the low-Fo olivine macrocrysts

The next question to address is how the high and low-Fo populations relate to each other. Trends in elements obtained only by EPMA (Ni, Mn, Cr, Fe, Mg) are qualitatively consistent with crystallisation of melt in equilibrium with the high-Fo population (e.g., higher Mn at lower Fo). Fractional crystallisation models reproduce well the relationships between Cr, Mn and Fo (Fig. 3b, f) but not with Ni (Fig. 3e), with the low-Fo population containing considerably more Ni than predicted by simple fractional crystallisation. This is not entirely surprising, given the evidence from previous studies showing that additional processes, such as melt mixing and diffusional re-equilibration contributed to the generation of Borgarhraun magmas (Stracke et al., 2003a; Maclennan et al., 2003a; Maclennan, 2008a, 2008b; Thomson and Maclennan, 2013). A variety of extra models were thus created to explain the Ni vs Fo relationship. The data were best reproduced by equilibrium crystallisation and melt-mixing, whereby the highest Fo primary melt composition was allowed to crystallise until equilibrium with $\sim Fo_{87}$, followed by mixing of this evolved melt with the original primary melt at varying proportions (Fig. 5a). Essentially, this simulates equilibrium crystallisation, followed by recharge, mixing and crystallisation. Despite the plausibility of explaining the major and minor element composition of the low-Fo population by coupled mixing and crystallisation of melts in equilibrium with high-Fo olivines, these same models are not capable of universally explaining the trace element data. Simple fractional crystallisation models can reproduce some trace element relationships (Fig. 4a, d, f, g) but fail at reproducing others (Fig. 4b, c, e, h, i). The equilibrium crystallisation and mixing models that explain the Ni-Fo data do not successfully reproduce Na-Y relationships (Fig. 5). Note that the equilibrium crystallisation and mixing models for Na-Y are very similar to simple fractional crystallisation models of the same data (Fig. 4h). We thus suggest that the parental melts of the low-Fo population follow a distinct magmatic lineage unrelated to the melts responsible for the high-Fo population. Although we can't discount that small amounts of melts from the high-Fo population mixed to form the low-Fo population, the trace element relationships demonstrate that it must have been volumetrically minor.

A remaining question to address is why the low-Fo olivines do not generally show trends in composition as shown by the high-Fo group. There are several possibilities. Firstly, the lower crust beneath northern Iceland is likely to be a complex amalgamation of the products of generations of magma injections, all of which have experienced variable cooling and crystallisation histories, and their crystal cargo subsequently intermingled (Maclennan et al., 2003a; Mutch et al., 2019a). Disaggregation of this crystal mush by fresh injections of melt would result in scavenging and mixing of different olivine populations that don't share a direct magmatic lineage. A second process to consider is sub-solidus modification during prolonged crustal storage. Thomson and Maclennan (2013), produced a model that showed how cumulate olivines, originally stratified by Fo content, are subsequently homogenised by diffusion. This produces increasingly a unimodal distribution of olivine compositions. Although most trace elements diffuse at similar rates to Fe-Mg in olivine, there are small differences (as can be seen in Figs. 5 and S1; Spandler and O'Neill, 2010; Tollan et al., 2015) which, with time, would lead to modification of the chemical trends formed through earlier differentiation. Disaggregation of such partially homogenised mushes would likely lead to a mixture of olivine macrocrysts without any clear petrogenetic relationship. We emphasise though that the model of Thomson and Maclennan (2013), whilst plausible to explain the trace element data of the low-Fo group, cannot explain compositional relationships the entire macrocryst population.

6.4. Relationship between olivine macrocrysts and carrier melt

All olivine macrocrysts show small (<50 μm) concentration profiles towards the crystal rim. Concentration profiles may be formed either through diffusion or crystal growth, and distinguishing between the two is crucial for correctly interpreting timescales of magmatic processes (Shea et al., 2015; Brenna et al., 2018; Mutch et al., 2019b). There are a number of options for discerning the relative contributions of these end-member processes. One option is to compare the concentration profiles of elements with greatly differing diffusion rates. Mutch et al. (2019b) utilised this

method for Borgarhraun olivines, taking slowly-diffusing Al as a monitor for the contribution from crystal growth. We could not take this approach, mainly due to the lack of any significant Al concentration profiles at the outermost 50 μm in the measured crystals. This in itself could potentially indicate diffusion as the dominant mechanism for generating the concentration profiles of the other elements. However, notable differences between the rim concentrations of these elements (e.g., Ni, Mn and Fo content) when compared with the data of Mutch et al. (2019b) indicates that the Borgarhraun olivines in our sample equilibrated with a different carrier liquid. An absence of a significant chemical potential gradient in Al would inhibit any concentration variation during growth or diffusion. There also remain questions regarding how much the rapid pathway of Al diffusion contributes to bulk Al diffusion in magmatic olivine (Zhukova et al., 2017; Le Losq et al., 2019), as discussed above. An alternative to Al is P (Shea et al., 2015), which is much slower diffusing and is unlikely to have a subsidiary fast mechanism (Spandler and O'Neill, 2010). Phosphorous profiles occasionally show variation in concentration in the outermost 50 μm, although correcting the profiles of rapidly diffusing elements using P and the approach of Mutch et al. (2019b) was not possible, since the rim concentrations of P vary significantly between crystals, and correlations between P and other elements are too inconsistent to generate linear growth curves (Mutch et al., 2019b). Instead, we tested the role of growth vs. diffusion by measuring approximately perpendicular profiles in the same crystals and then comparing the concentration profiles of anisotropically and isotropically-diffusing elements. In a diffusion-dominated system, the anisotropically-diffusing elements should show concentration profiles with different lengths, whereas the isotropically diffusing element profiles should be roughly the same. Fig. S6 (*Supporting online material*) shows a comparison between Cr, Mg-Fe, Y and P concentrations along two perpendicular profiles from two different crystals. Anisotropically- and rapid-diffusing elements (Cr, Mg-Fe) show different length scales in the two profiles (most apparent for Cr). Isotropically-diffusing Y shows nearly identical profiles in one crystal, and subtle differences in the second. Slow-diffusing P shows no correlation with the profiles of other elements, with only one profile showing any substantial variation in concentration towards the rim. In addition to the evidence from diffusive anisotropy, it is also difficult to reconcile such large compositional changes (Fo 90–78 and 4x increase in highly incompatible elements) occurring with such small amounts of rim overgrowth. Hence, while we cannot discount the possibility that growth played some role, we conclude that the concentration profiles of all elements (except P) are best explained through diffusion, rather than crystal growth.

Considering the profiles in detail (Fig. 7), two important observations are apparent: macrocrysts with high- and low-Fo compositions converge towards the same rim composition, and the rim composition for many elements is distinct from any of the macrocryst cores. The convergence of composition towards the rim is most distinct for Cr, Mn, Ni, Co and Fo content. Highly incompatible trace elements such as Ti and Y show more variance in rim composition. This is most likely due to a lack of precision in the profiles. Both Ti and Y have shorter profiles than other elements, resulting in a poorer model fit. In the case of Y, the concentrations are extremely low (<ppm), and hence there is additional uncertainty due to the less precise measurements. Nevertheless, the convergence of rim compositions clearly supports the hypothesis that a single more evolved melt scavenged the different populations of macrocrysts during ascent to the surface.

The Cr profiles provide even greater insight into the evolution of this transporting melt (Fig. 7a). Uniquely, low-Fo macrocrysts display sinusoidal Cr profiles, with a relatively steep increase in Cr concentration at the innermost rim, followed by a decrease in Cr concentration towards the interface, commensurate with the more Cr-rich macrocrysts. This initial steep increase is interpreted to reflect early re-equilibration with a transporting melt that was more primitive than the final erupted melt. We suggest that as the transporting melt ascended it continued to differentiate by fractional crystallisation of spinel and clinopyroxene, resulting in progressively decreasing equilibrium Cr concentrations (i.e., diffusion of Cr with a non-constant, decreasing activity of Cr at the crystal-melt interface). Similar effects may be anticipated for Ni and Mn due to olivine crystallisation, however the relative change in Ni and Mn is much smaller compared to Cr and thus not discernible in the measured concentration profiles.

This observation that Ni and Mn concentrations at the rim are distinct from any of the macrocryst cores, is even more apparent for highly incompatible trace elements. Yttrium, for example, has a final rim concentration ~4× higher than any of the macrocryst cores (Figs. 4 and 7). Assuming a representative $D^{olivine/melt}$ of 0.0036 (Mallmann and O'Neill, 2013), a melt in equilibrium with an olivine with 60 ppb would need to fractionally crystallise by approximately 74% to be in equilibrium with an olivine with ~250 ppb Y. Even greater amounts of crystallisation would be required to achieve this degree of enrichment considering that both plagioclase and clinopyroxene would also be liquidus phases, in which Y is more compatible than olivine. Such high degrees of differentiation are inconsistent with the relatively high-Fo content of the macrocryst rims ($Fo_{78–80}$), which requires only around 50% of fractional crystallisation of the least primitive of the two primary melt compositions based on PETROLOG calculations. Hence, we suggest that the carrier liquid is a distinctly different melt, unrelated directly to the melt from which the olivine macrocrysts crystallised.

6.5. Timescale of macrocryst transport

Diffusion profiles can also be used to estimate the time during which the macrocrysts were disaggregated and transported by the carrier melt. Ideally, the orientation of each profile relative to the principle crystallographic axes would be determined in order to precisely determine the diffusion timescale. Since crystal orientation was not measured here, we instead calculated the maximum and minimum times for each profile based on the anisotropy of the element in question (i.e., the maximum and minimum

diffusivities relative to the a, b and c axes). Although this is not as precise, it is still sufficient to distinguish timescales with approximately an order of magnitude difference (e.g., days from months).

The exercise used the same equation as above. In order to provide a tighter constraint, we performed the timescale calculation for multiple elements, namely Ni, Mn, Co, V, Ti, Y and Fe-Mg. The range of possible timescales was then constrained by the convergence of results. For this purpose we employed a temperature of 1200 °C, based on the PETROLOG calculations of the temperature of melt equilbrium with olivine Fo_{80} (the macrocryst rims). An oxygen fugacity of $\Delta FMQ = 0.3$ (where ΔFMQ is log units above the fayalite-magnetite-quartz oxygen buffer) at a pressure of 0.8 GPa (Gurenko et al., 1988) was calculated from the measured compositions of spinel inclusions and their host olivines, using the oxygen geobarometer of Ballhaus et al. (1991), with the correction of Ballhaus et al. (1994). It should be stressed that silica activity can also have a substantial effect on element diffusion in olivine (Jollands et al., 2016), which was not directly taken into account here, but should be similar to the experiments of Spandler and O'Neill (2010). The diffusion coefficients (D) for Fe-Mg were calculated from master equation (1) of Dohmen and Chakraborty (2007). These same values were also used for modelling the Mn profiles (Chakraborty, 2008). The values of D for Ni were calculated from Petry et al. (2004). For the remaining elements, we used the study of Spandler and O'Neill (2010). However, the diffusion coefficients from that study were only obtained at a single set of conditions ($T = 1300$ °C and $fO_2 = 10^{-3.3}$ Pa). To correct for this, we calculated the difference between the diffusion coefficient of Ni at the experimental conditions used by Spandler and O'Neill (2010) and the conditions of the diffusion model performed here (using the regressions of Petry et al., 2004). The resulting correction was a subtraction of 1.6 log units from the D_{Ni} values of Spandler and O'Neill (2010). This assumes that the dependence of Co, Ti, V and Y diffusion on temperature and fO_2 is similar to that of Ni, which is justified since the vacancy-controlled mechanism of diffusion for these elements in Fe-bearing olivine is the same (Spandler and O'Neill, 2010; Jollands et al., 2016). The success of this approach can be checked for Ni and Mn. Addition of 1.6 log units to the calculated D produces values of D_{Ni} which are within 0.2 log units of Spandler and O'Neill (2010). Manganese shows lesser agreement, with the differences of +0.2 and −0.4 log units for the slowest and fastest axes respectively relative to the values of Dohmen and Chakraborty (2007). The excellent agreement between Co timescales (calculated from the modified D of Spandler and O'Neill, 2010) and Fe-Mg, Mn and Ni timescales (all components which diffuse at very similar rates; Petry et al., 2004) demonstrates the efficacy of this approach.

Timescales calculated using Fe-Mg, Ni, Mn and Co yield a range of 70–250 days (Fig. 8). This relatively large range is due primarily to the measurement of concentration profiles relative to randomly sampled crystal orientations and morphologies. Timescales calculated for V, Ti and Y overlap with this range and extend to shorter timescales

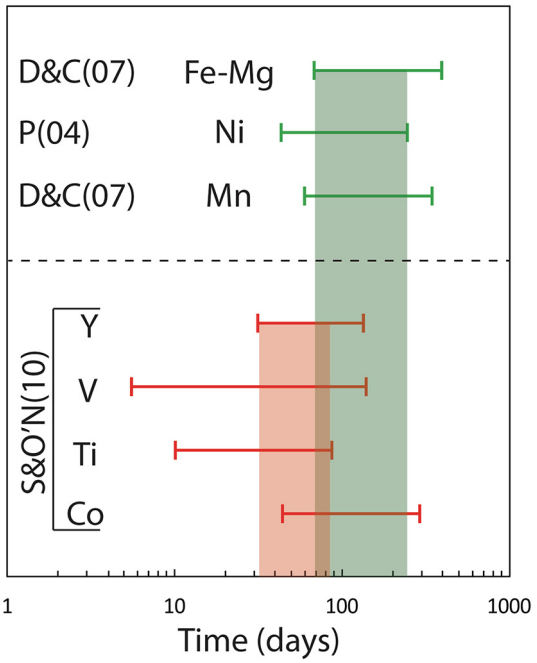

Fig. 8. Timescales calculated from diffusion modelling of LA-ICP-MS line profiles. The data for each element represents the range of values calculated from multiple profiles. Orientation of the profile relative to the crystal was not considered. Green values are calculated from diffusion coefficients specific for diffusion of that element at 1200 °C. Red values are calculated from diffusion coefficients produced experimentally at 1300 °C and subsequently corrected for the lower temperature. See discussion for a detailed explanation. The green and red shaded areas represent the range of timescales consistent with major/minor elements and incompatible trace elements respectively. References are as follows; D&C(07) is Dohmen and Chakraborty (2007), P(04) is Petry et al. (2004), S&O'N(10) is Spandler and O'Neill (2010).

(30–90 days). To a first order, this confirms that these elements are diffusing at a similar rate to major and minor components (Spandler and O'Neill, 2010; Tollan et al., 2015). The shift to generally shorter timescales may be an artefact of the greater uncertainty in the measured profiles of these trace elements relative to the better-constrained major and minor element concentrations, in addition to the uncertainty associated with the modified D values described above. However, it may also indicate that the chemical potential gradients of these elements are generated later during magmatic ascent, once more trace element-rich clinopyroxene begins to crystallise. Regardless, it is likely that the longer timescale of 70–250 days calculated from Fe-Mg, Ni and Mn are most reliable estimates for the total ascent history of the magma prior to eruption. These timescales are approximately an order of magnitude longer than those calculated for another sample from Borgarhraun by Mutch et al. (2019a, 2019b). It is important to note though, that there are significant differences between the two samples which may explain the discrepancy. Firstly, Mutch et al. (2019a, 2019b) report Al concentration profiles in their olivine macrocrysts, which we do not observe. Secondly, the rim concentrations of all elements are quite

different, with much lower Mg# and Ni and higher Mn in our olivine samples. Combined, this indicates that the Borgarhraun samples studied here were erupted by a different carrier liquid to those of Mutch et al. (2019a, 2019b), which would be consistent with the well-established heterogeneity within the lava flow (Stracke et al., 2003a; Maclennan et al., 2003a). Hence, the variation in eruption timescale is likely to reflect the episodic nature of magma recharge and eruption.

6.6. Relationship with matrix olivine

Two populations of fine-grained matrix (groundmass) olivine can be distinguished based on Fo content and NiO, MnO and TiO_2 concentrations (Fig. S3 – *Supplementary data*). Combined with the macrocryst compositions, this means that the total range of olivine compositions recorded within a single thin section is $Fo_{92–38}$, considerably greater than typically reported for basalts. The less evolved groundmass olivine population ($Fo_{67–80}$) overlaps with the rim composition of the olivine macrocrysts, indicating that the more primitive of these matrix olivines crystallised from the transporting melt with which the macrocrysts also partially equilibrated. The more evolved population ($Fo_{38–52}$ and up to 900 ppm Ti) however are not represented by any of the macrocryst rims. These compositions are typically found as thin (<10 μm) rims on interstitial growths of matrix olivine at the intersection of larger (50–200 μm) matrix crystals. We suggest that this highly evolved composition represents high degrees of fractionation of trapped interstitial melt. The near-absence of any quenched glass in the groundmass indicates that these highly evolved matrix phases grew by adcumulate growth, likely during slow cooling of the magma upon eruption. The inability to detect these evolved interstitial olivine compositions on the macrocryst rims indicates that this process of chemical differentiation during groundmass crystallisation was rapid relative to the transport-induced diffusion profiles. It is important to note that the groundmass crystallisation and the absence of glass observed in the sample studied here is distinctly different to the more rapidly quenched, glass-bearing samples reported in the majority of previous Borgarhraun studies (Maclennan et al., 2003a, 2003b; Thomson and Maclennan, 2013; Winpenny and Maclennan, 2011; Mutch et al., 2019a, 2019b), highlighting the substantial differences in lava flow texture which accompany whole-rock variations at Borgarhraun (Maclennan et al., 2003b). The extreme range of olivine compositions present on such a small spatial scale (<1 mm) is a stark demonstration of the challenges involved in understanding crystal-melt equilibrium in even seemingly primitive basalts, and the challenges presented in using whole rock compositions to understand the composition and crystallisation conditions of equilibrium parental melts.

6.7. Incompatible trace elements and the Icelandic mantle

The concentrations and ratios of incompatible trace and minor elements in olivine can reveal regional variations in the mantle beneath Iceland (Neave et al., 2018; Nikkola et al., 2019; Rasmussen et al., 2020). In Fig. 9, the ratios Ti/Y and Y/Zr in Borgarhraun olivines are compared with data from primitive (Háleyjabunga; $Fo_{88–90}$) and more evolved (Stapafell; $Fo_{85–88}$) Iceland lavas with dominantly peridotitic sources (Neave et al., 2018) and olivines from volcanic zones with proposed pyroxenite signatures (south Iceland volcanic zone and tertiary lavas: Rasmussen et al., 2020). Borgarhraun olivines are similar to olivines from Háleyabunga (Neave et al., 2018), with low Ti/Y and Zr/Y. Conversely, the data for olivines crystallising from melts were interpreted to have derived from garnet-bearing pyroxenite mantle have notably higher Ti/Y and Zr/Y (Rasmussen et al., 2020). Hence, the magmas feeding Borgarhraun most likely derived from a dominantly peridotitic, lower pressure (garnet-free) spinel-peridotite source (note that differences in the degree of partial melting may also have contributed to the fractionation of these trace element ratios). Comparisons can also be made with the olivine trace element dataset of Nikkola et al. (2019) who investigated lava flows from the south Iceland volcanic zone (Hvammsmúli and Brattaskjól) and central Iceland (Kistufell). Although Nikkola et al. (2019) did not measure Y or Zr, Ti concentrations give a good first order indication if the mantle source was relatively enriched or not. Olivine from Borgarhraun and Háleyjabunga (Neave et al., 2018) show similar Ti concentrations for a given Fo content (Fig. 9c), indicating a broadly similar mantle source, as inferred from Ti/Y and Zr/Y systematics. Olivines from all south Icelandic volcanic zone lavas (Hvammsmúli, Kistufell and, in particular, Brattaskjól) all have significantly higher Ti concentrations for the same Fo content (Nikkola et al., 2019), again in support of either a more fertile mantle source region, or extraction of smaller degree partial melts (Stracke et al., 2003a). These conclusions regarding differences in mantle source are broadly consistent with those deduced from radiogenic isotopes (Stracke et al., 2003a, 2003b). However, differences between the isotopic composition of Theistareykir lavas (including Borgarhraun) and those from elsewhere on Iceland point to subtle differences in mantle source that are not currently resolvable from olivine trace elements alone.

6.8. Chromium in olivine as a petrogenetic tool

A significant distinguishing feature of the Borgarhraun olivines is the very high Cr contents of the high-Fo macrocrysts, 400 ppm higher than olivines from any other Icelandic lava (Fig. 9). Paradoxically, Borgarhraun also has olivines with the lowest Cr contents of any Icelandic lava. These very low Cr contents (<100 ppm) occur at substantially higher Fo content than other Icelandic lavas ($Fo_{88–89}$ compared to $<Fo_{84}$), producing a unique, steep trend in Cr vs. Fo space compared to the rest of Iceland (Fig. 9d). Before addressing the causes of these differences, it is important to acknowledge the potential for a sampling bias. This could be due to either a lack of truly representative olivine data from other parts of Iceland, or due to an eruptive bias, whereby similarly Cr-rich olivines are formed in magmatic systems elsewhere on Iceland but simply not erupted. Furthermore, the data we present is all from the same lava

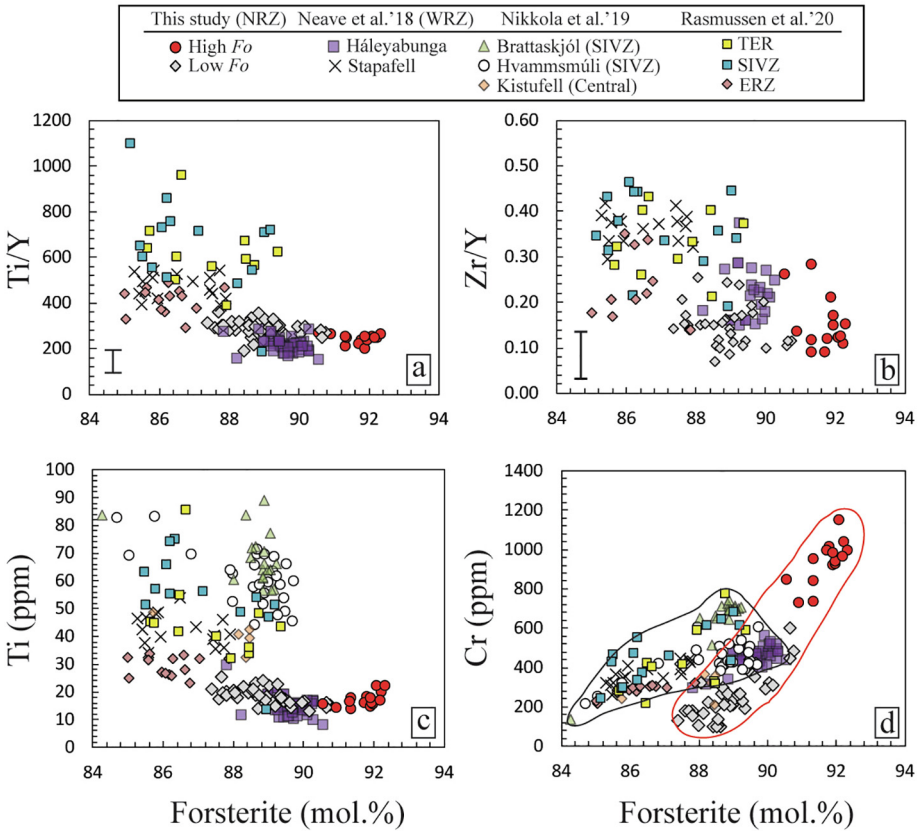

Fig. 9. Comparison of data from this study with data from Neave et al. (2018), Nikkola et al. (2019) and Rasmussen et al. (2020). 1sd uncertainty in trace element ratios is given by a black vertical bar in subfigures a and b. Note that in sub-Fig. 8b, concentrations of Y were in ppb rather than ppm. The trends of Fo vs. Cr for Borgarhraun and the rest of Iceland is outlined for clarity.

flow, whereas other studies report data from multiple flows within the same volcanic zone (Neave et al., 2018; Nikkola et al., 2019; Rasmussen et al., 2020). Assuming minimal sampling bias, the exceptionally high Cr contents at Borgarhraun may be due to unique mantle melting conditions, different olivine-melt partitioning behaviour or varying residual mantle mineralogy. Both temperature and melt composition may affect $D(Cr)^{ol/melt}$ (Hanson and Jones, 1998). However, from a compilation of literature partition coefficients over the temperature range of 1300–1400 °C and a broad array of melt compositions, $D(Cr)^{ol/melt}$ is expected to vary from 0.55 to 0.85 (Bell et al., 2014). This range in D values is unable to explain the difference in Cr contents of Borgarhraun macrocrysts and those from other lavas on Iceland. Variations in oxygen fugacity of crystallising melts are also an unlikely cause, since $D(Cr)^{ol/melt}$ is invariant over typical mantle fO_2 (Hanson and Jones, 1998; Mallmann and O'Neill, 2009; Bell et al., 2014). Residual mantle mineralogy could generate variations in melt Cr content, since Cr is considerably less compatible in garnet than in spinel (Roeder and Reynolds, 1991; Hauri et al., 1994). Thus, melting at higher pressures where garnet is increasingly stabilised relative to spinel should result in more Cr-rich melts. Differences in the amount of garnet in the mantle source may be apparent when comparing the REE patterns and MREE/HREE ratios of the Cr-rich and Cr-poor olivine populations, provided that the volume contribution of garnet melting is significant enough (Hauri et al., 1994; Johnson, 1998). Although the REE patterns appear nearly identical (Fig. 6), the ratio Dy/Lu does show a difference between the two macrocryst populations, with the most Cr-rich olivines having uniquely high values of Dy/Lu. This may indicate a small difference in the amount of melting in the garnet stability field, however, other Icelandic lavas with much stronger garnet signatures do not show such extreme Cr enrichments in olivine (Rasmussen et al., 2020). Hence, we consider variations in residual garnet and spinel to be relatively insignificant for explaining Borgarhraun olivine chemical variability. Having discounted partitioning and source mineralogy, the most plausible explanation for the Cr rich olivines is that the melts themselves had higher Cr contents. Roeder and Reynolds (1991) showed that for basaltic melt compositions, solubility of Cr increases by several tenths of wt.% as temperature increases from 1200 to 1400 °C. This change in solubility is similar to the difference in Cr content required in the crystallisation models in order to explain the range of Cr contents exhibited by the high-Fo macrocryst population (0.18 wt.% Cr_2O_3; Supplementary data).

Assuming again that previously published olivine data is representative of the respective magmatic systems, the contrastingly low Cr contents in the low-Fo Borgarhraun

population and the steepness of the trend in Cr vs. Fo compared to other Icelandic lavas (Fig. 9d) can be explained by the initial Cr contents and crystallisation pressure. High Cr melts result in early stabilisation of Cr-spinel relative to olivine, and hence a rapid depletion of Cr in the remaining melt with respect to decreasing Mg# during fractional crystallisation. Pressure of crystallisation is also important. Higher pressures of crystallisation result in the early appearance of clinopyroxene on the liquidus, as has been suggested for Borgarhraun lavas (0.8–1.0 GPa; Gurenko et al., 1988; Winpenny and Maclennan, 2011). Since Cr is compatible in clinopyroxene, such early crystallisation will result in Cr-rich compositions (>1 wt.% for Borgarharaun clinopyroxene; Maclennan et al., 2003a; Winpenny and Maclennan, 2011) which further deplete the residual melt in Cr during the early stages of differentiation. The effect of early, high pressure clinopyroxene crystallisation can be seen clearly in Fig. 3b and is also demonstrated in the supplementary data. Without early clinopyroxene crystallisation, the Cr content of olivine would be up to 350 ppm higher at around Fo_{87}, very similar to olivines from other Icelandic lavas (Fig. 9). Based on this relationship, it is possible that a large fraction of the substantial variation in Cr at a given Fo content may be due to pressure-induced variations in clinopyroxene crystallisation. Trends in Cr vs. Fo in olivine from different magmatic systems may therefore be a powerful tool for identifying variations in crystallisation pressures, with unusually steep trends (such as Borgarhraun) indicating an early period of deep crustal/upper mantle differentiation.

6.9. Re-envisaging the origin of the Borgarhraun lava flow

Although our conclusions regarding the origin of the Borgarhraun lava are overall consistent with previous studies (Maclennan et al., 2003a; Maclennan et al., 2003b; Maclennan, 2008a; Winpenny and Maclennan, 2011; Thomson and Maclennan, 2013), olivine trace elements provide an extra layer of detail on the mixing process. The key difference is that our new trace element data show a clear difference in the origin of the high and low-Fo olivine macrocryst groups, with simple near-binary melt mixing forming the former, and a more complex series of various parental melt compositions to form the latter. The melts forming the high-Fo population are unlikely to contribute significantly to melts forming the low-Fo population. Such a distinction is not indicated by either melt inclusions hosted by different olivine populations (Maclennan et al., 2003a), nor by clinopyroxene megacrysts from cumulate nodules (Winpenny and Maclennan, 2011). Olivine-hosted melt inclusions do show differences in La/Yb between the high and low-Fo group (Maclennan et al., 2003a). In addition, melt inclusions from the high-Fo population ($Fo_{90–92}$) show evidence for a decrease in the degree of melt mixing (based on REE ratios) with decreasing Fo content (Maclennan, 2008a). The new dataset reported here provides a slightly different view. Based on crystallisation models for a wide range of major, minor and trace elements in the olivine macrocrysts, the melt mixtures which generate the high-Fo population do not go on to crystallise the low-Fo population. Instead, we propose that these most primitive melt mixtures either stall at depth and erupt, or they are consumed by more voluminous evolved melts, diluting their presence in subsequent magma evolution. It should be emphasised that our conclusions here are based mainly on element concentrations rather than ratios, as used by previous studies (e.g., Maclennan et al., 2003a). Nevertheless, these near-binary mixing trends are still apparent in several incompatible element ratios, such as Dy/Lu (Fig. 6).

Another key difference is that based on the rim concentrations of most elements, particularly highly incompatible trace elements (Ti and Y), the carrier liquid is not only out of equilibrium with the macrocryst olivines (Maclennan et al., 2003a; Maclennan, 2008a; Winpenny and Maclennan, 2011; Thomson and Maclennan, 2013) but is furthermore not part of the same magmatic lineage. This is because the combination of Ti, Y and Fo contents at the rims are incompatible with fractional crystallisation of any of the modelled parental melt compositions. We thus suggest that disaggregation of the cumulate piles from which the macrocrysts came was triggered by fresh injections of a distinctly new melt. Chromium profiles uniquely show that this carrier liquid continued to differentiate during ascent to the surface. This process of melt injection, disagreggation and eruption was exceptionally quick (on the order of several months), based on modelling of diffusion profiles in the olivine macrocrysts. We should, however, also stress that the carrier liquid for this part of Borgarhraun is distinctly different from that sampled by previous studies, highlighted by the different olivine macrocryst rim compositions and groundmass textures (Maclennan et al., 2003b; Maclennan, 2008a, 2008b; Mutch et al., 2019b). This thus provides a further indication of the significant compositional heterogeneity present within the magmatic system feeding the eruption of the Borgarhraun lava.

7. CONCLUSION

Our study shows an example of how trace elements in olivine can be utilised to provide new insights into the behaviour of primitive mantle melts during early stages of differentiation. Highly forsteritic olivines, such as those measured here from Borgarhraun ($Fo_{90–92}$), are typically considered as proxies for near-primary melts. The trends observed in this study for trace elements, particularly Cr and highly incompatible elements such as Na and Y, demonstrate that even these highly magnesian melts can show clear evidence for melt mixing and concurrent crystallisation. A crucial point of our study is that models that reproduce relationships between major and minor elements (Fe, Mg, Mn and Ni) cannot consistently explain relationships involving trace elements. Relying solely on major and minor element data would thus have led to different and potentially erroneous conclusions. We envisage that such cryptic mixing trends may be regularly observed in the trace element concentrations of olivine phenocrysts which have otherwise subtle variations in major and minor element chemistry. High precision analysis of Cr, Na, Li, Ti and Y alongside other more commonly measured elements in

olivine, are therefore crucial for building a more detailed picture of how melts are generated and subsequently evolve once segregated from their mantle source.

Declaration of Competing Interest

The authors declare that they have no known competing financial interests or personal relationships that could have appeared to influence the work reported in this paper.

ACKNOWLEDGEMENTS

Pierre Lanari and Thomas Bovay are thanked for assistance with EPMA measurements. Two anonymous reviewers and the editor Andreas Stracke are thanked for their thorough and constructive reviews.

APPENDIX A

PETROLOG models

Fractional and equilibrium crystallisation models were constructed with PETROLOG using the two primary melt compositions described in Section 6. These melt compositions consist of the following components: SiO_2, TiO_2, Al_2O_3, FeO, Fe_2O_3, MnO, MgO, CaO, Na_2O and K_2O. The initial concentrations of the remaining elements included in the models (Cr, Y, Li, V) were calculated by taking the most and the least primitive olivines respectively from the high-Fo population and two sets of olivine-melt partition coefficients from Mallmann and O'Neill (2013). The first set of partition coefficients was from experiment C15/02/10, which was run at 1377 °C using a more primitive melt composition. The second set of partition coefficients was from experiment B15/03/11, which was run at 1300 °C using a less primitive melt composition. Both sets of experiments were conducted at atmospheric pressure. Note that the fO_2 of these two experiments were quite different (the former much more oxidising than the latter). With the exception of V, the olivine-melt partitioning behaviour of the elements modelled should not be affected by this (Mallmann and O'Neill, 2009; Bell et al., 2014). For V, the partition coefficients were calculated separately using equation (1) at FMQ and the temperatures of the two experimental runs. Note that neither of these experiments yielded partition coefficients for Na. Instead, partition coefficients were taken from other experiments at similar temperature, which best reproduced the maximum and minimum measured Na concentrations. Lithium was not included in the study of Mallmann and O'Neill (2013), so the value of 0.29 was taken from Spandler and O'Neill (2010). In the case of Ti, the TiO_2 of the starting melts is the same and the Ti partition coefficients from the two experiments are very similar. We thus modified the initial Ti concentration of the more evolved primary melt, from 0.7 wt.% to 0.4 wt.% in order to generate the maximum and minimum Ti concentrations in the high-Fo population. Likewise, the Ni and Mn concentrations of the starting melts were modified by calculating the Ni and Mn concentration of both end member melts. Nickel and Mn partition coefficients were calculated using Beattie et al. (1991).Partition coefficients for clinopyroxene-melt were taken from Le Roux et al. (2013) and McDade et al. (2003). A spinel-melt partition coefficient of 5 was used for V (Mallmann and O'Neill, 2009).

Fractional and equilibrium crystallisation calculations in PETROLOG using these starting compositions were performed at FMQ and a pressure of 0.8 GPa (Gurenko et al., 1988; Winpenny and Maclennan, 2011). The intermediate melt compositions in Figs. 3 and 5 were produced by mixing together primary melt compositions and differentiated melt compositions at different proportions. All calculations were stopped once an olivine composition of Fo_{87} was reached (the most evolved macrocryst composition found at Borgarhraun). The activity-composition models selected were from Ford et al. (1983) for olivine, Ariskin et al. (1993) for plagioclase and clinopyroxene and Ariskin and Nikolaev (1996) for spinel. In all of the models, spinel and olivine are the dominant phases early on, joined later by clinopyroxene and, finally, plagioclase. A major limitation of the model is the lack of a Cr component in clinopyroxene and the lack of a Mn component in both olivine and clinopyroxene. To account for Cr, the average Cr_2O_2 concentration of cumulate clinopyroxene from Maclennan et al. (2003a), 1.2 wt.%, was subtracted from the modelled melt composition at each? crystallisation step (using the % of clinopyroxene in the instantaneous crystallising assemblage calculated by PETROLOG; typically around 60%). A proper treatment of Cr in clinopyroxene is not available due to a lack of thermodynamic data for Cr-end member compositions. To model Mn the measured composition of olivine and spinel from this study and the average compositions of cumulate plagioclase and clinopyroxene (Maclennan et al., 2003a) were subtracted from the primary melt compositions. An intermediate composition of olivine chosen was from those documented in the supplementary information (Fo_{90}, MnO = 0.15 wt.%). The crystallising proportions were varied so that the modelled melt matched well the PETROLOG models for major elements, so that both the PETROLOG and the subtraction models were consistent with each other for common elements. This resulted in three stages of crystallisation: 1–6% was 95% olivine and 5% spinel, 7–13% crystallisation was 40% clinopyroxene, 57.5% olivine and 2.5% spinel, 14–20% crystallisation was 30% clinopyroxene, 20% olivine, 49.5% plagioclase and 0.5% spinel. Note that Fig. 3f only shows the results of modelling one primary melt compositions; the other melt compositions (primary and intermediate melts) show essentially identical results and hence are not included for clarity. The PETROLOG model also does not take into account Na in clinopyroxene, however, due to its incompatible nature, the effect on modelled Na concentrations is minor. A comparison of the two models is provided in the supplementary data.

APPENDIX B. SUPPLEMENTARY MATERIAL

Supplementary data to this article can be found online at https://doi.org/10.1016/j.gca.2020.07.033.

REFERENCES

Ariskin A. A., Frenkel M. Y., Barmina G. S. and Nielsen R. L. (1993) COMAGMAT: a fortran program to model magma differentiation processes. Computers & Geosciences 19, 1155-1170.

Ariskin A. A. and Nikolaev G. S. (1996) An empirical model for the calculation of spinel-melt equilibria in mafic igneous systems at atmospheric pressure: 1. Chromian spinels. *Contrib. Mineral. Petrol.* **123**, 282–292.

Baker D. R. (2008) The fidelity of melt inclusions as records of melt composition. *Contrib. Mineral. Petrol.* **156**, 377–395.

Ballhaus C., Berry R. F. and Green D. H. (1991) High-pressure experimental calibration of the olivine-orthopyroxene-spinel oxygen geobarometer: implications for the oxidation state of the upper mantle. *Contrib. Mineral. Petrol.* **107**, 27–40.

Ballhaus C., Berry R. F. and Green D. H. (1994) High-pressure experimental calibration of the olivine-orthopyroxene-spinel oxygen geobarometer: implications for the oxidation state of the upper mantle. *Contrib. Mineral. Petrol.* **118**, 109.

Beattie P., Ford C. and Russell D. (1991) Partition coefficients for olivine-melt and orthopyroxene-melt systems. *Contrib. Mineral. Petrol.* **109**, 212–224.

Bell A. S., Burger P. V., Le L., Shearer C. K., Papike J. J., Sutton S. R., Newville M. and Jones J. (2014) XANES measurements of Cr valence in olivine and their applications to planetary basalts. *Am. Mineral.* **99**, 1404–1412.

Bouvet de Maisonneuve C., Costa F., Huber C., Vonlanthen P., Bachmann O. and Dungan M. A. (2016) How do olivines record magmatic events? Insights from major and trace element zoning. *Contrib. Mineral. Petrol.* **171**, 56.

Brenna M., Cronin S. J., Smith I. E. M., Tollan P. M. E., Scott J. M., Prior D. J., Bambery K. and Ukstins I. A. (2018) Olivine xenocryst diffusion reveals rapid monogenetic basaltic magma ascent following complex storage at Pupuke Maar, Auckland Volcanic Field, New Zealand. *Earth Planet. Sci. Lett.* **499**, 13–22.

Bussweiler Y., Giuliani A., Greig A., Kjarsgaard B. A., Petts D., Jackson S. E., Barrett N., Luo Y. and Pearson D. G. (2019) Trace element analysis of high-Mg olivine by LA-ICP-MS-Characterization of natural olivine standards for matrix-matched calibration and application to mantle peridotites. *Chem. Geol.* **524**, 136–157.

Chakraborty S. (2008) Diffusion in solid silicates: a tool to track timescales of processes comes of age. *Annu. Rev. Earth Planet Sci.* **36**, 153–190.

Coogan L. A., Saunders A. D. and Wilson R. N. (2014) Aluminum-in-olivine thermometry of primitive basalts: Evidence of an anomalously hot mantle source for large igneous provinces. *Chem. Geol.* **368**, 1–10.

Costa F. and Dungan M. (2005) Short time scales of magmatic assimilation from diffusion modelling of multiple elements in olivine. *Geology* **33**, 837–840.

Danyushevsky L. V., Della-Pasqua F. N. and Sokolov S. (2000) Re-equilibration of melt inclusions trapped by magnesian olivine phenocrysts from subduction-related magmas: petrological implications. *Contrib. Mineral. Petrol.* **138**, 68–83.

Danyushevsky L. V., Leslie R. A. J., Crawford A. J. and Durance P. (2004) Melt inclusions in primitive olivine phenocrysts: The role of localized reaction processes in the origin of anomalous compositions. *J. Petrol.* **45**, 2531–2553.

Danyushevsky L. V. and Plechov P. (2011) Petrolog 3: Integrated software for modelling crystallization processes. *Geochem. Geophys. Geosyst.* **12**. https://doi.org/10.1029/2011GC003516.

Davidson J. P., Morgan D. J., Charlier B. L. A., Harlou R. and Hora J. M. (2007) Microsampling and isotopic analysis of igneous rocks: implications for the study of magmatic systems. *Annu. Rev. Earth Planet. Sci.* **35**, 273–311.

De Hoog J. C. M., Gall L. and Cornell D. H. (2010) Trace-element geochemistry of mantle olivine and application to mantle petrogenesis and geothermobarometry. *Chem. Geol.* **270**, 196–215.

Dohmen R. and Chakraborty S. (2007) Fe-Mg diffusion in olivine II: point defect chemistry, change of diffusion mechanisms and a model for calculation of diffusion coefficients in natural olivine. *Phys. Chem. Minerals* **34**, 409–430.

Dungan M. A. and Davidson J. P. (2004) Partial assimilative recycling of the mafic plutonic roots of arc volcanoes: an example from the Chilean Andes. *Geology* **32**, 773–776.

Feig S. T., Koepke J. and Snow J. E. (2010) Effect of oxygen fugacity and water on phase equilibria of a hydrous tholeiitic basalt. *Contrib. Mineral. Petrol.* **160**, 551–568.

Foley S. F., Prelevic D., Rehfeldt T. and Jacob D. E. (2013) Minor and trace elements in olivines as probes into early igneous and mantle melting processes. *Earth Planet. Sci. Lett.* **363**, 181–191.

Ford C. E., Russell D. G., Craven J. A. and Fisk M. R. (1983) Olivine-liquid equilibria: temperature, pressure and composition dependence of the crystal/liquid cation partition coefficients for Mg, Fe2+, Ca and Mn. *J. Petrol.* **24**, 256–266.

Gerasimovsky V. I., Polyakov A. I. and Durasova H. F., et al. (1978) *Iceland and the Mid-Atlantic Ridge, Geokhemistry*. Nauka, Moscow, pp. 184 (in Russian).

Gurenko A. A., Sobolev A. V., Polyakov A. I. and Kononkova N. N. (1988) Primary melt of rift tholeiites of Iceland: composition and conditions of crystallization. *Transactions (Doklady) of the USSR Academy of Sciences* **301**, 109–113 (Translated from: Pervichnyy rasplav riftogennykh toleitov Islandii: sostav i uslovia kristallizatsii. *Doklady Akademii Nauk. SSSR* **301**, 179–184).

Hanson B. and Jones J. H. (1998) The systematics of Cr^{3+} and Cr^{2+} partitioning between olivine and liquid in the presence of spinel. *Am. Mineral.* **83**, 669–684.

Hauri E. H., Wagner T. P. and Grove T. L. (1994) Experimental and natural partitioning of Th, U, Pb and other trace elements between garnet, clinopyroxene and basaltic melts. *Chem. Geol.* **117**, 149–166.

Heinonen J. S., Jennings E. S. and Riley T. R. (2015) Crystallisation temperatures of the most Mg-rich magmas of the Karoo LIP on the basis of Al-in-olivine thermometry. *Chem. Geol.* **411**, 26–35.

Herzberg C. (2011) Identification of source lithology in the Hawaiian and Canary Islands: Implications for origins. *J. Petrol.* **52**, 113–146.

Jennings E. S., Gibson S. A. and Maclennan J. (2019) Hot primary melts and mantle source for the Paraná-Etendeka flood basalt province: New constraints from Al-in-olivine thermometry. *Chem. Geol.* **529**, 119287.

Jochum K. P., Willbold M., Raczek I., Stoll B. and Herwig K. (2005) Chemical characterisation of the USGS reference glasses GSA-1G, GSC-1G, GSD-1G, GSE-1G, BCR-2G and BIR-1G using EPMA, ID-TIMS, ID-ICP-MS and LA-ICP-MS. *Geostand. Geoanal. Res.* **29**, 285–302.

Jochum K. P., Weis U., Stoll B., Kuzmin D., Yang Q., Raczek I., Jacob D. E., Stracke A., Birbaum K., Frick D. A., Günther D. and Enzweiler J. (2011) Determination of Reference Values for NIST SRM 610–617 glasses following ISO guidelines. *Geostand. Geoanal. Res.* **35**, 397–429.

Johnson K. T. M. (1998) Experimental determination of partition coefficients for rare earth and high-field-strength elements between clinopyroxene, garnet and basaltic melt at high pressures. *Contrib. Mineral. Petrol.* **133**, 60–68.

Jollands M. C., Padrón-Navarta J. A., Hermann J. and O'Neill H. St. C. (2016) Hydrogen diffusion in Ti- doped Fo and the preservation of metastable point defects. *Am. Mineral.* **101**, 1571–1583.

Kent A. J. R. (2008) Melt inclusions in basaltic and related volcanic rocks. *Rev. Mineral. Geochem.* **69**, 273–331.

Le Losq C., Jollands M. C., Tollan P. M. E., Hawkins R. and O'Neill H. St. C. (2019) Point defect populations of Fo revealed by two-stage metastable hydroxylation experiments. *Contrib. Mineral. Petrol.* **174**, 53.

Le Roux V., Dasgupta R. and Lee C. A. (2013) Recommended mineral-melt partition coefficients for FRTEs (Cu), Ga, and Ge during mantle melting. *Am. Mineral.* **100**(11-12), 2533–2544.

Maclennan J., McKenzie D., Hilton F., Gronvöld K. and Shimizu N. (2003a) Geochemical variability in a single flow from northern Iceland. *J. Geophys. Res.* **108**. https://doi.org/10.1029/2000JB000142.

Maclennan J., McKenzie D., Grönvold K., Shimizu N., Eiler J. M. and Kitchen N. (2003b) Melt mixing and crystallization under Theistareykir, northeast Iceland. *Geochem. Geophys. Geosyst.* **4**. https://doi.org/10.1029/2003GC000558.

Maclennan J. (2008a) Concurrent mixing and cooling of melts under Iceland. *J. Petrol.* **49**, 1931–1953.

Maclennan J. (2008b) Lead isotope variability in olivine-hosted melt inclusions from Iceland. *Geochim. Cosmochim. Acta* **72**, 4159–4176.

Mallmann G. and O'Neill H. St. C. (2009) The crystal/melt partitioning of V during mantle melting as a function of oxygen fugacity compared with some other elements (Al, P, Ca, Sc, Ti, Cr, Fe, Ga, Y, Zr and Nb). *J. Petrol.* **50**, 1765–1794.

Mallmann G. and O'Neill H. St. C. (2013) Calibration of an empirical thermometer and oxybarometer based on the partitioning of Sc, Y and V between olivine and silicate melt. *J. Petrol.* **54**, 933–949.

Matthews S., Shorttle O. and Maclennan J. (2016) The temperature of the Icelandic mantle from olivine-spinel aluminum exchange thermometry. *Geochem. Geophsy. Geosyst.* **17**, 4725–4752.

McDade P., Blundy J. D. and Wood B. J. (2003) Trace element partitioning on the Tinaquillo Lherzolite solidus at 1.5 GPa. *Phys Earth Planet. Int.* **139**, 129–147.

Mutch E. J. F., Maclennan J., Holland T. J. B. and Buisman I. (2019a) Millenial storage of near-Moho magma. *Science* **365**, 260–264.

Mutch E. J. F., Maclennan J., Shorttle O., Edmonds M. and Rudge J. F. (2019b) Rapid transcrustal magma movement under Iceland. *Nat. Geosci.* **12**, 569–574.

Neave D. A., Passmore E., Maclennan J., Fitton G. and Thordarson T. (2013) Crystal-melt relationships and the record of deep mixing and crystallization in the AD 1783 Laki eruption, Iceland. *J. Petrol.* **54**, 1661–1690.

Neave D. A., Shortle O., Oeser M., Weyer S. and Kobayashi K. (2018) Mantle-derived trace element variability in olivine and their melt inclusions. *Earth Planet. Sci. Lett.* **483**, 90–104.

Nikkola P., Guðfinnsson G. H., Bali E., Rämö O. T., Fusswinkel T. and Thordarson T. (2019) Signature of deep mantle melting in South Iceland olivine. *Contrib. Mineral. Petrol.* **174**, 43.

O'Neill H. St. C. and Jenner F. E. (2012) The global pattern of trace-element distributions in ocean floor basalts. *Nature* **491**, 698–704.

Palme H., O'Neill H. St. and C. (2003) Cosmochemical estimates of mantle composition. *Tr Geo* **2**, 568.

Paton C., Hellstrom J., Paul B., Woodhead J. and Hergt J. (2011) Iolite: Freeware for the visualisation and processing of mass spectrometric data. *J Anal. Atom. Spec.* **26**, 2508–2518.

Petry C., Chakraborty S. and Palme H. (2004) Experimental determination of Ni diffusion coefficients in olivine and their dependence on temperature, composition, oxygen fugacity, and crystallographic orientation. *Geochim. Cosmochim. Acta* **68**, 4179–4188.

Polyakov A. I., Ilyin N. P. and Muravyeva N. S. (1976) Conditions of crystallization of rocks of Iceland rhyolite-basalt association on basis of studying composition of phenocrysts and distribution coefficients. *Geokhimiya* **7**, 963–982 (in Russian).

Rasmussen M. B., Halldórsson S. A., Gibson S. A. and Guðfinnsson G. H. (2020) Olivine chemistry reveals compositional source heterogeneities within a tilted mantle plume beneath Iceland. *Earth Planet. Sci. Lett.* **531**, 116008.

Roeder P. L. and Reynolds I. (1991) Crystallization of chromite and chromium solubility in basaltic melts. *J. Petrol.* **32**, 909–934.

Ruprecht P. and Plank T. (2013) Feeding andesitic eruptions with a high-speed connection from the mantle. *Nature* **500**, 68.

Shea T., Lynn K. J. and Garcia M. O. (2015) Cracking the olivine zoning code: Distinguishing between crystal growth and diffusion. *Geology* **43**, 935–938.

Shorttle O. and Maclennan J. (2011) Compositional trends of Icelandic basalts: Implications for short-length scale lithological heterogeneity in mantle plumes. *Geochem. Geophys. Geosyst.* **12**. https://doi.org/10.1029/2011GC003748.

Shorttle O., Moussallam Y., Hartley M. E., Maclennan J., Edmonds M. and Murton B. J. (2015) Fe-XANES analyses of Reykjanes Ridge basalts: implications for oceanic crust's role in the solid Earth oxygen cycle. *Earth Planet. Sci. Lett.* **427**, 272–285.

Slater L., McKenzie D., Grönvold K. and Shimize N. (2001) Melt generation and movement beneath Theistareykir, NE Iceland. *J. Petrol.* **42**, 321–354.

Sobolev A. V., Hofmann A. W., Kuzmin D. V., Yaxley G. M., Arndt N. T., Chung S.-L., Danyushevsky L. V., Elliott T., Frey F. A., Garcia M. O., Gurenko A. A., Kamenetsky V. S., Kerr A. C., Krivolutskaya N. A., Matvienkov V. V., Nikogosian I. K., Rocholl A., Sigurdsson I. A., Shushchevskaya N. M. and Teklay M. (2007) The amount of recycled crust in the sources of mantle-derived melts. *Science* **316**, 412–417.

Sobolev A. V., Asafov E. V., Gurenko A. A., Arndt N. T., Batanova V. G., Portnyagin M. V., Garbe-Schönberg D. and Krasheninnikov S. P. (2016) Komatiites reveal a hydrous Archaean deep-mantle reservoir. *Nature* **531**, 628.

Spandler C., O'Neill H. St. C. and Kamenetsky V. S. (2007) Survival times of anomalous melt inclusions from element diffusion in olivine and chromite. *Nature* **447**, 303–306.

Spandler C. and O'Neill H. St. C. (2010) Diffusion and partition coefficients of minor and trace elements in San Carlos olivine at 1,300°C with some geochemical implications. *Contrib. Mineral. Petrol.* **159**, 791–818.

Spice H. E., Fitton J. G. and Kirstein L. A. (2016) Temperature fluctuation of the Iceland mantle plume through time. *Geochem. Geophys. Geosyst.* **17**, 243–254.

Stead C. V., Tomlinson E. L., Kamber B. S., Babechuk M. G. and McKenna C. A. (2016) Rare earth element determination in olivine by laser ablation-quadropole-ICP-MS: an analytical strategy and applications. *Geostand. Geoanal. Res.* **41**, 1–16.

Stracke A., Zindler A., Salters V. J. M., McKenzie D., Blichert-Toft J., Albarède F. and Grönvold K. (2003a) Theistareykir revisited. *Geophys. Geosyst. Geochem.*. https://doi.org/10.1029/2001GC000201.

Stracke A., Zindler A., Slaters V. J. M., McKenzie D. and Grönvold K. (2003b) The dynamics of melting beneath

Theistareykir, northern Iceland. *Geophys. Geosyst. Geochem.*. https://doi.org/10.1029/2002GC000347.

Thomson A. and Maclennan J. (2013) The distribution of olivine compositions in Icelandic basalts and picrites. *J. Petrol.* **54**, 745–768.

Tollan P. M. E., O'Neill H. St. C., Hermann J., Benedictus A. and Arculus R. J. (2015) Frozen melt-rock reaction in a peridotite xenolith from sub-arc mantle recorded by diffusion of trace elements and water in olivine. *Earth Planet. Sci. Lett.* **422**, 169–181.

Tollan P. M. E., O'Neill H. St. C. and Hermann J. (2018) The role of trace elements in controlling H incorporation in San Carlos olivine. *Contrib. Mineral. Petrol.* **173**, 89.

Wan Z., Coogan L. A. and Canil D. (2008) Experimental calibration of aluminum partitioning between olivine and spinel as a geothermometer. *Am. Mineral.* **93**, 1142–1147.

Winpenny B. and Maclennan J. (2011) A partial record of mixing of mantle melts preserved in Icelandic phenocrysts. *J. Petrol.* **52**, 1791–1812.

Zhukova I., O'Neill H. and Campbell I. H. (2017) A subsidiary fast-diffusing substitution mechanism of Al in Fo investigated using diffusion experiments under controlled thermodynamic conditions. *Contrib. Mineral. Petrol.* **172**, 53.

Associate editor: Andreas Stracke